

---

Masters Theses

Student Theses and Dissertations


---

Summer 2018

## Research and development of optically transparent join with low processing temperatures

Eric Kevin Muskovin

Follow this and additional works at: [https://scholarsmine.mst.edu/masters\\_theses](https://scholarsmine.mst.edu/masters_theses)

 Part of the [Inorganic Chemistry Commons](#), and the [Materials Science and Engineering Commons](#)  
Department:

---

### Recommended Citation

Muskovin, Eric Kevin, "Research and development of optically transparent join with low processing temperatures" (2018). *Masters Theses*. 7805.  
[https://scholarsmine.mst.edu/masters\\_theses/7805](https://scholarsmine.mst.edu/masters_theses/7805)

This thesis is brought to you by Scholars' Mine, a service of the Missouri S&T Library and Learning Resources. This work is protected by U. S. Copyright Law. Unauthorized use including reproduction for redistribution requires the permission of the copyright holder. For more information, please contact [scholarsmine@mst.edu](mailto:scholarsmine@mst.edu).

RESEARCH AND DEVELOPMENT OF OPTICALLY TRANSPARENT JOIN  
WITH LOW PROCESSING TEMPERATURES

by

ERIC KEVIN MUSKOVIN

A Thesis

Presented to the Faculty of the Graduate School of the  
MISSOURI UNIVERSITY OF SCIENCE AND TECHNOLOGY

In Partial Fulfillment of the Requirements for the Degree  
MASTER OF SCIENCE IN MATERIAL SCIENCE AND ENGINEERING

2018

Approved by

William G. Fahrenholtz, Advisor  
Richard K. Brow  
Jeffrey D. Smith

© 2018

ERIC KEVIN MUSKOVIN

ALL RIGHTS RESERVED

## **PUBLICATION THESIS OPTION**

This thesis consists of the following two articles, formatted in the style used by the Missouri University of Science and Technology:

Paper I: Pages 24-49 are intended for submission to Thin Solid Films

Paper II: Pages 50-72 are intended for submission to The Journal of Sol-Gel Science and Technology

## ABSTRACT

The purpose of this study was to investigate durable solar cell cover glass joins produced by diffusion bonding with deep eutectic solvents (DES) and to develop a novel process of joining optically transparent materials at low temperatures. A joined PV cell-glass specimen was characterized using Raman,  $\mu$ -FTIR, SEM-EDS, and thin-film XRD. DESs were created with malonic acid (MAL) and choline chloride (ChCl) of varying composition factors (CF;  $CF = \text{MAL}/\text{ChCl}$ ). Joining borosilicate glass coupons was attempted using DESs with  $CF = 0.65$  and  $1$  at temperatures between  $100$ - $150$  °C for 20 hours. Joining the glass coupons failed at all temperatures and oxygen partial pressures. Metal salts and borosilicate glass solubilities were studied in a DES with varying CF. Oxide solubilities increased as CF approached  $1$ .  $\text{AlCl}_3$ ,  $\text{Al}(\text{NO}_3)_3$ , and silicic acid exhibited greater solubilities than their corresponding oxides, but were not sufficient for joining.

Silica was dissolved in a choline hydroxide (ChOH)-methanol solution to produce a join between borosilicate glass coupons at low temperatures. Tetramethoxysilane (TMOS) and hexamethyldisilazane (HMDS) were added as network modifiers. Thermal analyses showed alcohol condensation reactions occur at  $67$  °C. A solid join was produced between two borosilicate glass coupons when held at  $67$  °C for 20 hours. Optical spectroscopy showed the join had  $>80\%$  transmission in the range of  $350$ - $1100$  nm. The joins were thermally stable at  $70$  °C, but the decomposition of ChOH caused discoloration at  $>80$  °C.

## ACKNOWLEDGEMENTS

This research was funded by the Air Force Research Laboratory (FA9453-14-D-0312) through a sub-contract with ATA Corporation (purchase order 160300).

I would like to thank Dr. William Fahrenholtz for advising me and providing funds for the project.

I would also like to thank Dr. David Wilt and Dr. Jessica Buckner of the AFRL Space Vehicles Directorate, and Dr. Bernie Carpenter of Aerospace Corporation for their technical guidance.

I acknowledge the use of the Advanced Materials Characterization Laboratory at MS&T. I would also like to thank Dr. Eric Bohannon and Ron Haas for their help with the operation of equipment.

## TABLE OF CONTENTS

	Page
PUBLICATION THESIS OPTION.....	iii
ABSTRACT.....	iv
ACKNOWLEDGEMENTS.....	v
LIST OF ILLUSTRATIONS.....	x
LIST OF TABLES.....	xiii
 SECTION	
1. INTRODUCTION.....	1
2. LITERATURE REVIEW.....	6
2.1. DEEP EUTECTIC SOLVENTS.....	6
2.2. SOL-GEL PROCESSING.....	9
2.2.1. Silica Chemistry.....	13
2.2.2. Dependence on the Surface Area/Size.....	14
2.2.3. Polymerization pH Dependence.....	15
2.2.4. Organic Bases.....	16
2.3. ORGANIC-INORGANIC HYBRIDS.....	17
2.4. WAFER JOINING TECHNIQUES.....	18
2.4.1. Glass Frit Joining.....	18
2.4.2. Spin-On Glass Joining.....	20
2.4.3. Polymer Adhesive Joining.....	21
2.4.4. Eutectic Joining.....	22

## PAPER

I. RESEARCH AND DEVELOPMENT OF DURABLE SOLAR CELL COVER GLASS BONDING.....	24
ABSTRACT.....	24
1. INTRODUCTION.....	24
2. EXPERIMENTAL PROCEDURE.....	25
2.1. DES PREPARATION.....	25
2.1.1. Characterization.....	26
2.1.2. Dissolution of Metal Salts.....	26
2.2. JOINED GLASS-PV CELL CHARACTERIZATION.....	27
2.3. JOINING GLASS SLIDES.....	28
2.4. COPPER-ALUMINA JOINING.....	29
2.4.1. Characterization.....	29
3. RESULTS AND DISCUSSION.....	29
3.1. DES CHARACTERIZATION.....	29
3.2. DISSOLUTION OF METAL SALTS.....	32
3.3. JOINED GLASS-PV CELL CHARACTERIZATION.....	35
3.4. JOINING GLASS SLIDES.....	41
3.5. JOINING $Al_2O_3$ WITH CU INTERLAYERS.....	43
4. CONCLUSIONS.....	47
REFERENCES.....	49
II. LOW TEMPERATURE JOINING OF BOROSILICATE GLASS UTILIZING CHOLINE HYDROXIDE.....	50



ABSTRACT.....	50
1. INTRODUCTION.....	50
2. EXPERIMENTAL PROCEDURE.....	52
2.1. LIQUID PRECURSOR PREPARATION.....	52
2.2. BONDING.....	53
2.3. THERMAL STABILITY.....	54
2.4. CHARACTERIZATION.....	54
3. RESULTS AND DISCUSSION.....	55
3.1. DSC/TGA CHARACTERIZATION.....	55
3.1.1. Liquid Precursors.....	55
3.1.2. Bonded Specimen.....	62
3.2. RAMAN SPECTROSCOPY.....	64
3.3. UV-VIS CHARACTERIZATION.....	66
3.4. ISOTHERMAL HOLDS.....	69
4. CONCLUSIONS.....	70
REFERENCES.....	71

## SECTION

3. CONCLUSIONS.....	73
3.1. PAPER I CONCLUSIONS.....	73
3.2. PAPER II CONCLUSIONS.....	74
3.3. OVERALL CONCLUSIONS.....	74
4. SUGGESTIONS FOR FUTURE WORK.....	75
4.1. THERMAL STABILITY.....	75

4.2. MECHANICAL TESTING.....	75
BIBLIOGRAPHY.....	77
VITA.....	83

## LIST OF ILLUSTRATIONS

Figure	Page
<b>Section</b>	
1.1. Schematic of IMM cross-section before inversion, illustrating differences in band gap energies between semiconductor layers.....	1
2.1. The minimum melting temperatures of dicarboxylic acid-choline chloride mixtures occurs at 50 mol% acid.....	8
2.2. Choline hydroxide is an unstable molecule that will decompose at ambient temperature.....	9
2.3. Cubic octasilicate ions contain eight terminal sights on the corners of the cubes.....	17
2.4. The addition of PDMS influences the network and elastic properties of ormosils.....	19
<b>Paper I</b>	
1. DSC analysis of DES (CF=1) between -50 °C to 50 °C.....	30
2. DTA analysis between 20 °C and 340 °C of DES (CF=0.65), MAL, and ChCl under argon.....	31
3. TGA analysis between 20 °C and 340 °C of DES (CF=0.65), MAL, and ChCl under argon. The black line denotes the mass ratio of MAL:ChCl (MAL = 54%, ChCl = 46%).....	32
4. The effect of CF, oxidation state of Cu, and presence of Al and Si ions on Cu ion concentration. Points without error bars have errors smaller than the point size.....	34
5. Cross-section of a joined PV cell showing the PV cell (top), join layer (middle), and cover glass (bottom).....	36

6.	Image showing the location for EDS (spectrum 5) of the join layer taken near the interface with the PV cell.....	37
7.	$\mu$ -FTIR spectra of the joined PV cell specimen and background atmosphere.....	39
8.	Raman spectra of cross-sectioned joined PV cell using a He-Ne laser source (632.8 nm).....	40
9.	Thin film XRD pattern of the join layer from a separated PV cell-cover glass specimen.....	40
10.	Image of oxidized copper and alumina pieces before joining.....	44
11.	Image of Al <sub>2</sub> O <sub>3</sub> specimen after heating.....	44
12.	Image of separated Al <sub>2</sub> O <sub>3</sub> after heating illustrating the region of interaction where copper foil and alumina were in contact.....	45
13.	SEM image and EDS maps of cross-sectioned of separated Cu-Al <sub>2</sub> O <sub>3</sub> specimen.....	46
14.	SEM image and the composite EDS map of the surface where the copper foil was in contact with the alumina.....	47

## Paper II

1.	DSC/TGA of choline hydroxide-silica solution in air.....	56
2.	DSC/TGA data of CM liquid precursor.....	57
3.	DSC/TGA analyses of CMH liquid precursor.....	59
4.	Comparison of DSC analyses for CM and CE precursors.....	59
5.	TGA analyses of CM and CE precursors.....	60
6.	DSC analyses of CMH and CEH precursors.....	62

7.	TGA analyses of CMH and CEH precursors.....	63
8.	DSC analyses of CMH liquid (CMH_L) and CMH solid (CMH_S).....	64
9.	TGA analysis of CMH liquid (CMH_L) and CMH solid (CMH_S).....	65
10.	Raman spectra of CMH solid and CMH liquid; alkoxy silane peaks at 525, 589, and 609 $\text{cm}^{-1}$ (green), 3-dimensional silica network peaks at 830 and 1080 $\text{cm}^{-1}$ (orange).....	66
11.	Schematic representation of cross-linking structures and corresponding Raman vibrational modes .....	67
12.	Specimen bonded with CMH liquid precursor at 67 °C.....	67
13.	An optical micrograph of the center of the specimen joined with CMH liquid at 67 °C.....	68
14.	UV-Vis spectra of CMH bonded glass and two unbonded coverglass slides.....	68
15.	Bonded specimens after 1-hour isothermal holds at specified temperature.....	69

**LIST OF TABLES**

Table	Page
Paper I	
1. Concentrations of dissolved metal species (in ppm) in DES mixtures at different CFs.....	33
2. Concentrations metal ions (in ppm) produced from metal salts in DES with CF=1.....	36
3. Atomic concentrations measured by spot EDS (Spectrum 5) for the join layer.....	37
4. Possible vibrational modes characteristic of the measured $\mu$ -FTIR peaks.....	39
Paper II	
1. Molar ratios of components in liquid precursors.....	53

## 1. INTRODUCTION

Inverted metamorphic multi-junction photovoltaic cells (IMMs) are solar cells consisting of several layers of semiconducting materials with descending band gap energies (Figure 1.1).



Figure 1.1. Schematic of IMM cross-section before inversion, illustrating differences in band gap energies between semiconductor layers<sup>1</sup>.

IMMs have better energy conversion properties than conventional gallium arsenide and germanium-based multi-junction solar cells<sup>1</sup>. They also provide a higher efficiency with a smaller mass than conventional crystalline solar cells which decreases the total mass in a solar array. The low weight, high efficiency properties makes IMMs ideal candidates for satellite applications. To prevent

damage from solar radiation, the IMM is joined to a thin sheet of cerium-doped borosilicate glass<sup>2</sup>. Joining the two substrates requires a process that fits within certain thermal, mechanical and optical parameters that cannot be satisfied by conventional joining techniques.

Compared to traditional solar cells, IMM is less rigid and is prone to cracking under mechanical stress. The glass sheet that covers the cells adds some rigidity, but the glass is kept thin to reduce the overall weight of the cell. IMM can survive temperature excursions up to 400 °C, but they cannot be held at these elevated temperatures longer than a few minutes without significant damage. The final join must also have a coefficient of thermal expansion (CTE) close to the IMM and borosilicate glass to minimize thermal stresses during the joining process and normal operation. To maintain the IMM efficiency, the join must have high transmission (greater than or equal to the protective coverglass) in the optical wavelength range. Due to the UV-absorption properties of the cerium-doped glass, the optical characteristics at shorter wavelengths do not impact performance.

The conventional technique used to join solar cells to protective glass uses adhesives, specifically optical silicone. Adhesive joining is a low temperature joining technique (<450 °C) that employs the use of polymers and epoxies to bond two substrates. The problems with adhesive joining IMM to the protective cover glass are that the cured join has a low elastic modulus (50 MPa) and the coefficient of thermal expansion (CTE) ( $275 \times 10^{-6} \text{ }^\circ\text{C}^{-1}$ , Dow Corning MS1000-2 Moldable Silicone) is much greater than the substrates, which could



lead to delamination or distortion. Optical silicones have curing temperatures below 120 °C, but the final join has a relatively low rigidity which can lead to strain on the protective glass and solar cell. A large strain on the glass and solar cell can cause cracking and mechanical failure. Thermosetting polymers are more rigid but require high temperatures (~450 °C) to soften enough for joining<sup>3</sup>, which damages the IMMs if left for extended periods of time.

Glass frit bonding provides desirable mechanical characteristics and the resulting join can produce an intermediate CTE that minimizes thermal stresses. The thermal and mechanical characteristics are due to the inorganic bonds in the glass structure, which are much stronger than hydrogen-bonded polymers<sup>4</sup>. However, the temperature required to join the substrates without crystallizing the glass frit exceeds the survivable temperature of the IMMs. Based on this assessment, none of the typical joining techniques provides the combination of processing temperature and final properties needed for IMM solar cell applications.

Sol-gel processing can produce inorganic layers at lower temperatures than conventional glass frit bonding while maintaining desirable thermal and mechanical characteristics for IMM-cover glass joining. The problems with sol-gel materials stem from the volatilization of the solvent and products from the hydrolysis and condensation reactions. The loss of gaseous species produces in a large volume shrinkage that can cause stress cracking and voids within the join<sup>5</sup>. If the substrates are not permeable, the volatilized species within the join will cause the voids to expand and separate the cover glass from the IMM.

To reduce the total volume shrinkage, this project utilizes a choline hydroxide-methanol solution to increase the total silica concentration in the starting solution. Increasing the silica concentration of the starting solution reduces the concentration of volatiles, which reduces the volume shrinkage that occurs when transitioning from solution to final product. However, volume contraction still occurs during the curing process and can still cause stress cracking.

Hexamethyldisilazane (HMDS) can be added to silica-based networks to allow the silica molecules to move freely during volume contraction and reduce the probability of stress fracture. HMDS terminates a fraction of the reactive silica species that would otherwise create inorganic bonds between silica units<sup>6</sup>.

The objective of this project is to develop a process to produce a bond between two borosilicate glass substrates that meets the desired characteristics for solar cell applications. The process should produce a bond at low temperatures (<300 °C) that has high optical transmission (>80% transmission at 350-700 nm). The resulting bond should have a sufficient strength so that the glass substrates cannot be easily separated. The bond should be temperature stable up to 150 °C: the bond should remain solid, optically transparent, and bonded to the substrates. It is assumed that the bond will require a silica content that is as high as possible to achieve a bond that fits within the parameters.

This project investigated the use of deep eutectic solvents as a means of diffusion bonding the borosilicate glass substrates. The deep eutectic solvents can partially dissolve the glass substrates, which changes the chemistry of the

solvent. The increase in silica concentration should increase the melting temperature of the solvent and has the potential of producing a solid bond under isothermal conditions as the silica content of the bond layer increases.

This project also investigated a low temperature sol-gel process as a possible bonding process. The sol-gel process utilized silica dissolved in an organic base to increase the silica concentration compared to conventional sol-gel processes. The organic base also acted as a catalyst for condensation reactions at low temperatures producing a solid bond.

## 2. LITERATURE REVIEW

The following literature review contains background information on deep eutectic solvents, sol-gel processing, silica chemistry, organic-inorganic hybrids and wafer bonding techniques. A deep eutectic solvent was used in the preliminary process as a novel way to produce optically transparent bonds for borosilicate glass. The second process is a low temperature sol-gel process that relies on the dissolution chemistry of silica in a strong organic base, so it is important to review the basics of sol-gel and silica chemistry. The second process produces an organic-inorganic hybrid material with a high silica concentration. Finally, this review contains information on current wafer bonding techniques to show the advantages and disadvantages of each technique related to this work.

### 2.1. DEEP EUTECTIC SOLVENTS

Deep eutectic solvents (DESs) are non-aqueous ionic liquids that consist of a halide salt, which is a hydrogen bond acceptor (HBA), and a hydrogen-bond donor (HBD) such as an acid. Separately, the HBA and the HBD are solid, having melting temperatures above room temperature. When mixed, the HBA and HBD undergo a solid-state reaction that decreases the melting point of the mixture<sup>7</sup>. At a certain concentration, the mixture will be at its eutectic point, which is the minimum melting temperature in the system.

A particularly interesting class of DESs is based on of choline chloride and a carboxylic acid. Choline chloride is a quaternary ammonium halide salt ( $C_5H_{14}ClNO$ ) with a decomposition temperature of 302 °C. It was once thought that choline chloride and carboxylic acid underwent a chemical reaction forming liquid hydrochloric acid. However, that chemical reaction would produce a choline salt with the remaining carboxylic ion that would be solid at room temperature; since no solids were present at the completion of the reaction, this chemical reaction is unlikely. In choline chloride, the negatively charged chloride ion is loosely attracted to the positively charged ammonium end of the structure. The hydroxyl groups on the carboxylic acid attract the chloride ion to the point where it is shared between the two molecules. This charge delocalization causes the melting temperature of the complex molecule to decrease. To form the eutectic, two carboxylic groups are required for each chloride ion. For monocarboxylic acids, the eutectic occurs at 66.7 mol % acid; for dicarboxylic acids like oxalic acid, it occurs at 50 mol % acid. The melting temperature depression of the carboxylic acid-choline chloride mixtures at eutectic compositions is large (Figure 2.1): in the oxalic acid ( $T_m=190$  °C)-choline chloride ( $T_m=302$  °C) system, the melting temperature of the mixture is decreased by 212 °C compared to a melting temperature 246 °C that would be predicted by linear interpolation between the two end members<sup>8</sup>.

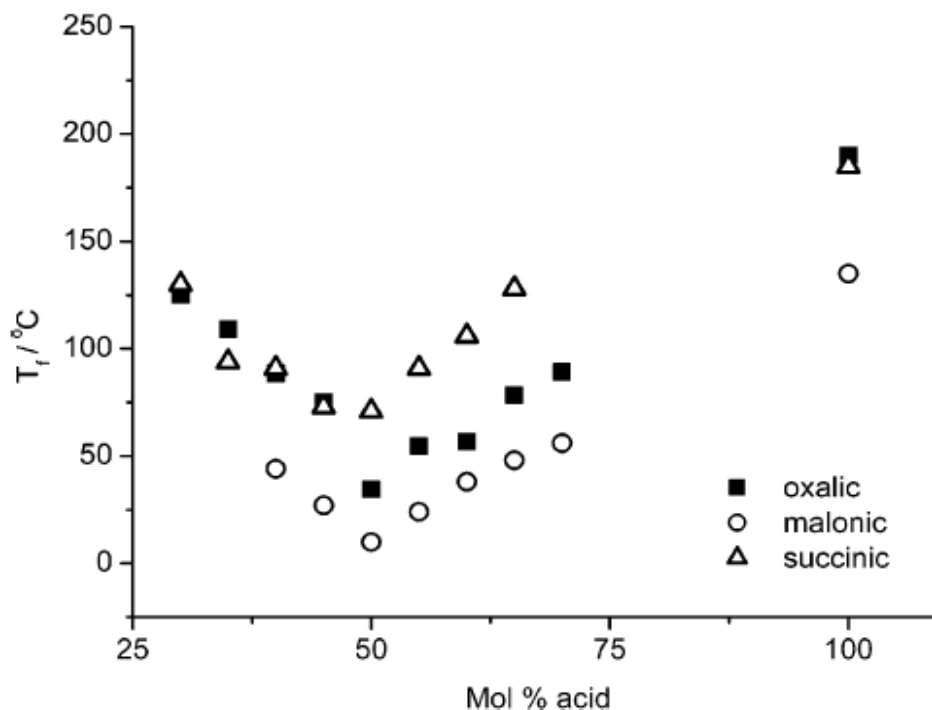


Figure 2.1. The minimum melting temperatures of dicarboxylic acid-choline chloride mixtures occurs at 50 mol% acid<sup>8</sup>.

The delocalized chloride ion makes DESs exceptional solvents for metal oxides, forming chloride complexes with the metal cations<sup>9–11</sup>. The solubility of the metal oxides is dependent on the ionic character; more covalent oxides are less susceptible to form a chloride complex and have a lower solubility in the DESs<sup>12</sup>. Metal oxides with high percent ionic character, such as CuO and ZnO, show higher solubilities in choline chloride-based DESs due to their propensity to form the chloride complexes.

The ability to dissolve inorganic materials makes DESs suitable solvents for synthesizing inorganic materials. The thermal characteristics of DESs have distinct advantages over traditional solvents: their low melting temperature allows

for the synthesis of materials to occur at lower processing temperatures, and their high thermal stability allows for a wide range of operating temperatures<sup>13</sup>. DESs are attractive for metallic electrochemical deposition because of their high electrical conductivities<sup>14</sup>. However, choline chloride-based DESs have questionable electrochemical stability as any water present in the solution will reduce at the cathode and form choline hydroxide<sup>15</sup>. Choline hydroxide undergoes a Hoffman elimination reaction (Figure 2.2) at ambient temperature, volatilizing trimethylamine and vinyl alcohol.

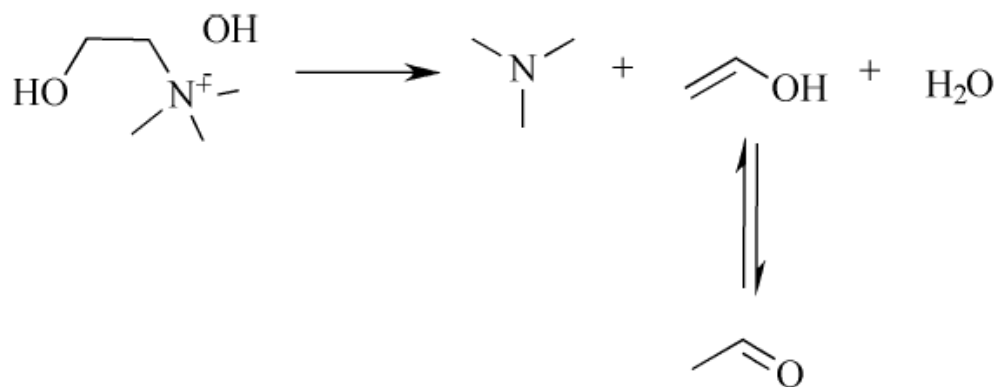


Figure 2.2. Choline hydroxide is an unstable molecule that will decompose at ambient temperature<sup>15</sup>.

## 2.2. SOL-GEL PROCESSING

Sol-gel processing is the process of synthesizing inorganic materials from precursors in solution<sup>16</sup>. The precursors in solution polymerize by means of a condensation reaction, linking the precursor molecules and releasing a smaller

molecule. If the precursor molecule can make two bonds, the molecules will polymerize to form long chain-like polymers; if the molecules can form more than two bonds, they will polymerize to form a 3-dimensional network eventually forming a macroscopic molecule. Once the macroscopic molecule is large enough to span the volume of the solution, the product is considered a gel. At a certain point, the solution will reach its gel point, which is the time it takes for the precursors to polymerize into a large 3-dimensional network with unreacted solution trapped within the network. At the gel point, the network is compliant allowing unreacted sections to move closer to each other to condense further. The process of condensation after the gel point is called aging. The solvent and the by-products are removed from the solution through a drying process, producing a fully linked inorganic network called a xerogel or dry gel<sup>16</sup>.

The most commonly used precursors in sol-gel processing are metal alkoxides<sup>16</sup>. Metal alkoxides are molecules that contain a metal-oxygen-hydrocarbon bond. Due to their high electronegativity, the oxygen-hydrocarbon (alkoxy) bond is susceptible to condensation reactions<sup>17, 18</sup>. Metal alkoxides will produce metal hydroxides in the presence of water through a process known as hydrolysis. When another metal alkoxide is near the hydroxyl groups, the alkoxy groups condense to form a metal-oxygen-metal bond and an alcohol by-product. If two metal hydroxides condense, they form a metal-oxygen-metal bond and a water molecule as the by-product.

The rate of condensation reactions can be influenced by the pH of the solution before gelation. When an acid is present, it acts to protonate the



alkoxide group of the precursor molecule leaving behind a metal cation<sup>19</sup>. The cation hydrolyzes, forming a metal hydroxide much faster than a standard hydrolysis reaction. In a basic solution, the hydroxyl ion deprotonates metal hydroxides to form a nucleophilic metal-oxide species<sup>20</sup>. If the hydroxyl ion comes into close proximity to an alkoxy species, similarly, it will bond with the alkyl species to produce a corresponding alcohol and leave a metal-oxide nucleophile. In base-catalyzed reactions, the solvent has a much greater effect on the hydrolysis reaction than in acid-catalyzed reactions<sup>16, 21</sup>.

Condensation reactions are reversible under the right conditions; these reverse reactions are known as reesterification. Reesterification is more prevalent in acidic rather than basic systems due to their mechanisms of condensation reactions. Reesterification also depends on the chemical nature of the solvent and the concentration throughout the condensation process. In acidic environments, a high concentration of higher-order alcohol will make the thermodynamically unfavorable reesterification reaction more favorable, resulting in a product with high organic content<sup>22</sup>. However, if methanol is the solvent, reesterification is not thermodynamically favorable in any condition and it is not dependent on concentration.

In the presence of water vapor, gels can adsorb water. Water can only be adsorbed on hydroxylated surface silica units and not siloxane bonds as siloxane bonds are largely hydrophobic<sup>23, 24</sup>. Rehydration is temperature dependent as the number of residual hydroxylated silica bonds decreases as temperature increases<sup>25, 26</sup>. The decrease in hydroxylated silica is due to the increased

hydroxylation reactions at high temperatures<sup>27, 28</sup>. At temperatures below 400 °C, the hydroxyl concentration is sufficient for water adsorption to happen readily. However, heating a fully hydroxylated silica gel to 400 °C changes the nature of the silica surface and the number of hydroxyl sites that can be rehydrated starts to decrease<sup>29</sup>.

After the three-dimensional gel has been formed, excess solvent and unreacted precursors are removed through a drying process. At first, the sol undergoes drying at a rate that is independent of time, the constant rate period (CRP). The CRP starts with constant evaporation of liquid from the surface of the body: the rate of evaporation is proportional to the difference between the vapor pressure of the liquid and the ambient vapor pressure. After the liquid completely evaporates from the body's surface, menisci form at the surface of pores open to the atmosphere. The body begins to shrink from the capillary tension formed from the evaporation of liquid within the pore. Initially, stresses in the shrinking body are negligible as the body is compliant because the network is not completely cross-linked. However, during the drying process, new bonds form between unreacted groups and the porosity decreases, which increases the rigidity of the body. Eventually, the rigidity is large enough to overcome the capillary tension and volume shrinkage stops, which is known as the critical point. The liquid withdraws into the pores and the rate of evaporation starts to decrease. This point marks the end of the CRP and the start of the falling rate period (FRP). During the FRP, the evaporation of liquid is largely affected by the flow of fluid to the surface of the body. The vapor pressure on the outside surface

is still lower than the pressure inside the pores. The resulting pressure gradient forces the liquid up the sides of the pores to the surface where it evaporates<sup>30</sup>. As the liquid-vapor interface recedes further into the gel, the vapor pressure gradient decreases resulting in a decrease in the evaporation rate. Differences in volume shrinkage through the body can cause pressure gradients, which give rise to drying stresses. For thick gels and high drying rates, the surface dries and contracts much faster than the center of the gel resulting in large drying stresses. As gels increase in thickness, the drying stresses increase; thick gels are more prone to fracture due to drying stresses<sup>16</sup>.

Silylation is the reaction that replaces a hydroxyl group with an organosilyl group (a silicon bonded to an organofunctional group)<sup>31</sup>. Additions of organosilyl groups have shown to improve hydrophobicity in silica materials produced by sol-gel processes<sup>6, 32, 33</sup> and by chemical vapor deposition<sup>34, 35</sup>. Increasing the organic content in siliceous materials decreases the density, so organosilicon-modified silica thin films are often used for anti-reflective coating applications. Organosilyl groups are unreactive groups, they rarely form bonds between two silica molecules. When used in a sol-gel process, organosilyl groups terminate reactive hydroxyl groups allowing the silica network to rearrange and relax easily during the drying process. Therefore, adding organosilyl groups reduces the amount of stress in the final product<sup>36</sup>.

**2.2.1. Silica Chemistry.** The rate of dissolution of amorphous silica has a strong dependence on the pH of the solvent. Hydroxyl ions can penetrate the open silica structure due to their relatively small size. Hydroxyl ions hydrolyze

surface silica units producing soluble silica species that go into solution. In solution where the hydroxyl concentration is high ( $\text{pH} > 11$ ), the hydrolyzed silica species react with the hydroxyl ions in solution to form colloidal silica and water. This reaction decreases the concentration of the hydrolyzed silica at the surface allowing the silica to dissolve continuously. In solutions with an intermediate hydroxyl concentration ( $3 < \text{pH} < 11$ ), the hydrolyzed silica remains in solution and the rate of dissolution is controlled by the hydroxyl concentration. Hydrofluoric acid is a unique case: although its concentration of hydroxyl ions is low, the rate of silica dissolution in hydrofluoric acid is similar to that of a strong base. The fluoride ions are similar in size to hydroxyl ions and, therefore, can also fit in the amorphous silica structure. This means that the dissolution of silica is also dependent on the atomic-level structure. However, the effects of fluoride ions and hydroxyl ions are not identical; fluoride ions require a proton to dissolve silica<sup>20</sup>.

**2.2.2. Dependence on the Surface Area/Size.** The rate of silica dissolution is proportional to the specific surface area of the silica particles. However, silica particles with a diameter less than 5 nm do not follow this proportionality because they exhibit a much higher solubility than larger particles. Silica particles with diameters less than 5 nm have more than 50% of its Si atoms on the surface. Therefore, the particles must have one or more silanol bonds.

Silanol bonds may be protonated or deprotonated, depending on the pH of the solution. If the pH is greater than the point of zero charge (PZC), silanols deprotonate and the particle surface becomes negatively charged; if the pH is less than the PZC, the silanols protonate and the surface becomes positively

charged. The surface charges lead to an electrostatic repulsion between particles, preventing particles from aggregating and flocculating. If the attractive forces and the electrostatic repulsion between particles are in balance, the colloids remain in suspension and the sol stabilizes<sup>16</sup>.

**2.2.3. Polymerization pH Dependence.** The pH dependence of silica polymerization can be broken down into three ranges:  $\text{pH} < 2$ ,  $2 < \text{pH} < 7$ , and  $\text{pH} > 7$ . Silica has a point of zero charge at pH 2 where the surface charge of silica particles equals zero. This is also the isoelectric point of silica or the point at which a particle carries no net electrical charge. During polymerization, the silica monomer can be expressed as an anion at  $\text{pH} > 2$ , with a net negative charge<sup>20</sup>. Hydroxyl ions are the catalyst for dissolution of silica at a  $\text{pH} > 2$ , therefore the negative catalyst ions make the silica anionic. The abundance of protons in a solution with a  $\text{pH} < 2$  causes silica monomers to protonate, producing a net positive charge and surfaces that are considered largely cationic<sup>37</sup>. In between these two pH ranges, there exists a point of temporary maximum colloid stability where the anionic monomers and cationic monomers are in equilibrium, the isoelectric point. At the isoelectric point, silica experiences a minimum point of gelling as the monomers are at their most stable point and polymerization is at its relative minimum. Since the silica particles are at their smallest and the growth rate is at its slowest, the surface area and strength of the gel are at a maximum at pH 2.

Between pH 2 and pH 7, the polymerization of silica is slow, and the polymeric units and particles have no charge. During the early stages, silica

nuclei (2-3 nm) form and aggregate into interconnected particle chains and three-dimensional silica networks.

In solutions with a pH >7, polymerization is spontaneous and fast: in similar conditions, a silica gel will form in minutes at pH 8 and in hours at pH 2. When silica monomers link to form oligomers, the pKa value of the molecules decreases from 9.9 and approaches 6.7 as the molecules become larger. Due to the fewer hydroxyl groups resulting from condensation reaction, the overall acidity of the silica increases. The remaining hydroxyl group of the three dimensional network are more ionized and will preferentially bond with monomers in solution resulting in rapid spontaneous polymerization<sup>20</sup>. The ending product are macroscopic particles and their size is largely temperature dependent. Due to their surface charges, the particles experience charge repulsion preventing aggregation. The process temperature controls the “Ostwald ripening”, or the growth of larger particles at the expense of smaller ones. Higher temperatures increase the solubility of the small particles in solution, causing the larger particles to grow.

**2.2.4. Organic Bases.** Silicate species can be prepared using a sufficiently strong organic base. Quaternary ammonium hydroxides (QAHs) are strong organic bases (pH >13) that exhibit high silica solubility. Unlike strong mineral bases, QAHs don't allow hydrolyzed silica or ionic silica species to equilibrate in solution. In a tetramethylammonium hydroxide (TMAH) solution, the hydroxide penetrates the silica structure and hydrolyzes the surface silica like that of a strong base. The hydroxyl ions form colloidal silica, but due to the

negative charge of the colloid surfaces, positively charged tetramethylammonium ions are adsorbed on the surfaces, which stabilizes silica colloids<sup>38</sup>.

Quaternary ammonium ions affect silicate ions, resulting in the formation of silicate cage-like structures. Tetramethylammonium ions and choline ions produce cubic octameric silicate ions ( $\text{Si}_8\text{O}_{20}^{4-}$ ), a double four-membered ring with oxygen ions as the terminal sites<sup>39</sup>, as shown in Figure 2.3.

### 2.3. ORGANIC-INORGANIC HYBRIDS

Organic-inorganic (O-I) hybrid materials are composite materials containing both inorganic and organic components. Additions of organic components to inorganic materials can lead to considerable changes in optical<sup>41</sup>,<sup>42</sup> and mechanical<sup>43</sup> properties. O-I hybrids can be synthesized at low temperatures through solvolysis and sol-gel processing techniques<sup>44</sup>.

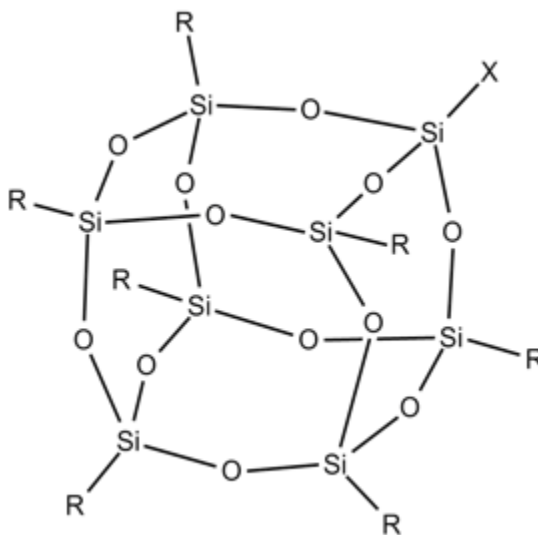


Figure 2.3. Cubic octasilicate ions contain eight terminal sites on the corners of the cubes<sup>40</sup>.

Ormosils are a class of O-I hybrid where the organic component may be bonded to a silica network. Ormosils can be synthesized using alkoxysilanes and silylating network modifiers with a sol-gel processing technique. The modified silica product from the sol-gel process can vary in mechanical properties depending on the network structure and the ratio of organic and inorganic compositions<sup>45</sup> (figure 2.4). Organic species can be incorporated into a silica network by functionalizing an organic polymer with groups that hydrolyze during the sol-gel process or by combining with polymers that contain a functional group. Hexmethyldisilazane (HMDS) is a trimethylsilylating agent that can be used to produce antireflective ormosils. HMDS has an advantage over other silylating agents because it can silylate reactive functional groups, like alkoxysilane and silanol groups, in situ during the sol-gel process<sup>42</sup>. Polydimethylsiloxanes (PMDS) can be added to alkoxysilanes to produce ormosils with long polymeric chains inside an inorganic network. Small amounts of PMDS can produce an ormosil at room temperature with relatively high hardness. However, hardness and elastic modulus values decrease drastically at higher concentrations of PMDS<sup>46</sup>. The ease of property modification makes ormosils a viable material for a variety of applications.

## **2.4. WAFER JOINING TECHNIQUES**

**2.4.1. Glass Frit Joining.** Glass frit joining uses a low melting temperature glass as an intermediate bonding layer. The glass frit, or vitrified glass powder, is placed between two substrates and heated to its wetting



temperature. The wetting temperature is the temperature at which the viscosity is low enough for the glass to flow and wet the surface of the substrates. As the glass wets the substrate surfaces, it forms a bond at an atomic level and, when cooled, produces a mechanically strong bond<sup>47</sup>.

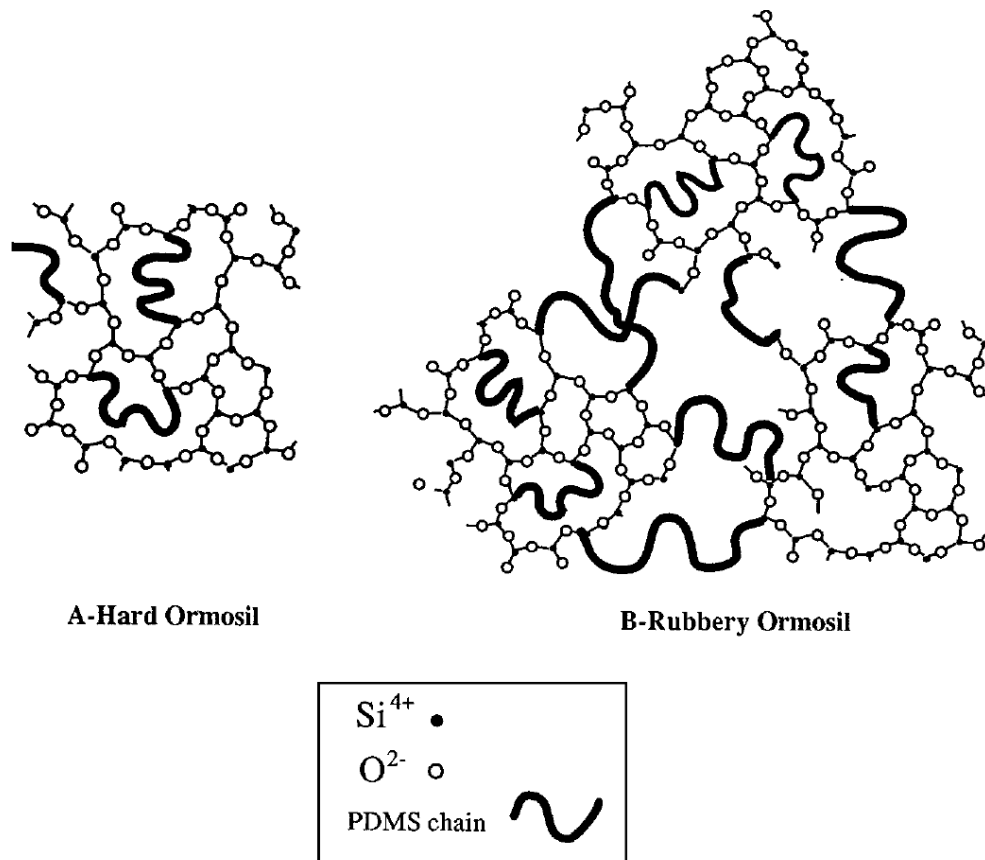


Figure 2.4. The addition of PDMS influences the network and elastic properties of ormosils<sup>46</sup>.

Joining with glass frit requires a low melting temperature glass; wafer joining requires a processing temperature below 450 °C<sup>48</sup>. Lead and lead-silicate glasses are typically used in glass frit joining due to their low melting

temperatures and optical transparency<sup>48–50</sup>. Typically, low melting temperature glasses have a higher thermal expansion coefficient (CTE) than glasses with higher melting temperatures. Increasing the amount of PbO in a silicate glass decreases the glass transition temperature and increases the CTE<sup>49, 51</sup>. Filler glasses with higher melting temperatures are added to the lead silicate glass frit to reduce the CTE closer to the substrate CTE. Matching the CTEs reduces the stress at the substrate-glass-frit interface<sup>47</sup>.

**2.4.2. Spin-On Glass Joining.** Spin-on glass (SOG) is a gel with a viscosity that allows a thin layer to be deposited onto a substrate using centripetal force. The deposited gel is sandwiched by another substrate and a force can be applied perpendicular to the gel layer decreasing the layer thickness. Solvents are removed through a low temperature baking step which increases the viscosity of the gel. Finally, the gel is cured at a higher temperature that results in a fully reacted inorganic join. SOGs have lower processing temperatures compared to other bonding techniques that produce inorganic bonds. Silicate SOGs can be fully cured around 400 °C, but can produce a sufficient bond at 200 °C<sup>52</sup>. The final join should show exceptional crack resistance<sup>53</sup>, thermal stability, and adhesion to the substrates<sup>54</sup>. Depending on layer thickness, the join can contain low stress; a thick layer develops more drying stresses than a thin layer. Silicate SOGs are useful for bonding two materials with large differences in CTE because they can compensate the mechanical stress induced by thermal change<sup>54</sup>. However, sufficiently thick

substrates must be used to prevent warping from volume shrinkage during the baking step.

**2.4.3. Polymer Adhesive Joining.** Polymer adhesive joining uses an intermediate polymer to join two materials. The polymers used to join can be placed into four categories: thermosetting polymers, thermoplastic polymers, elastomers, and hybrid polymers. Thermosetting polymers start as a liquid polymeric precursor with long polymeric chains. When heated, the polymeric chains crosslink to produce a three-dimensional network and form a solid join that cannot be re-melted or reshaped. Thermoplastic polymers are solid at room temperature and can be re-melted. Joining with thermoplastic polymers involves melting or softening the polymer at elevated temperatures between two substrates. The thermoplastic polymer solidifies when cooled below its melting temperature and produces a solid join. Elastomers are viscoelastic polymers that can endure large deformations at low stresses. Joining with elastomers is similar to thermosetting polymeric joining as they are both applied as a liquid and are solidified into an irreversible bond. Hybrid polymers are combinations of two or more polymers of the former categories. The characteristics and the joining process of the hybrid polymers vary based on the type of polymer combination<sup>55</sup>. All four types of polymers can be used in joining materials<sup>56</sup>.

Typically, polymers adhere well to many substrate materials. Polymer cohesion is a result of van der Waals bonding between the polymeric molecules and the surface of the substrate. Forming van der Waals bonds requires a small distance (<0.5 nm) between the opposing atoms<sup>57</sup>. Therefore, the polymer used

to join must have exceptional wetting characteristics with the substrate to produce a strong join.

Joining polymers have relatively low thermal stability compared to inorganic joining materials. Thermoplastic polymers can survive temperatures above 200 °C for short periods of time but can deform or melt at higher temperatures. Thermosetting polymers are significantly more rigid than thermoplastic polymers at relatively high temperatures (>200 °C) and can survive temperatures up to 450 °C. However, thermosetting polymers have relatively low bond strength compared to thermoplastic polymers. Elastomers have the lowest thermal stability and can only survive temperatures less than 260 °C<sup>56, 58, 59</sup>.

Joining brittle substrates requires a rigid join with a high elastic modulus to avoid substrate fracture under load. Compared to inorganic joining materials, polymers have lower elastic modulus values. Generally, thermosetting polymers have higher elastic moduli than thermoplastic polymers and elastomers. Elastic modulus values for common thermosetting polymers typically range from 2-30 GPa while thermoplastic polymers range from 0.1-5.5 GPa. Elastomers have the lowest elastic modulus of the three polymer categories, with values ranging from 1-19 MPa<sup>60</sup>.

**2.4.4. Eutectic Joining.** Eutectic joining is the process of joining two dissimilar materials by the formation of a eutectic alloy containing components from the original materials. The materials are placed into direct contact and heated to a temperature between the liquidus temperature and the melting temperature of the substrates. A liquid forms from the reaction between the two

materials and can form a solid join when cooled below the liquidus temperature<sup>61</sup>. Due to the similarity in chemistry to the substrates, the eutectic liquid has exceptional wettability to the substrate surfaces and produces a strong bond<sup>62</sup>. Atomic diffusion of components can change the local composition of the eutectic liquid near the substrates that can increase the melting temperature. Holding the system at constant temperature can cause solidification of the join if the composition change increases the melting temperature above the isothermal temperature<sup>63</sup>.

## PAPER

### I. RESEARCH AND DEVELOPMENT OF DURABLE SOLAR CELL COVER GLASS BONDING

ERIC MUSKOVIN AND WILLIAM FAHRENHOLTZ

MISSOURI UNIVERSITY OF SCIENCE AND TECHNOLOGY

#### ABSTRACT

Deep eutectic solvents (DESs) were investigated to form diffusion bonds between borosilicate glass coupons at temperatures below 200 °C. The solubility of silica in DES was not adequate to produce a bond. Varying temperature and oxygen concentration did not have a significant effect on the success of the join. A specimen joined using DESs was analyzed and characterized as a silicon-based organic-inorganic hybrid. A previously studied copper-alumina diffusion bonding process was investigated to understand the mechanics of diffusion bonding.

#### 1. INTRODUCTION

Deep eutectic solvents (DESs) are a class of ionic solvents consisting of two salts that exhibit a large decrease in melting temperature at the eutectic composition<sup>1</sup>. Metal oxides with high percent ionic character show high

solubilities in DESs<sup>2</sup>. The ability to dissolve inorganic materials makes DESs suitable solvents for synthesizing inorganic materials.

Diffusion bonding is a technique to join inorganic materials at temperatures lower than the melting temperatures of the substrates. Previous studies have shown that copper can be utilized to produce mechanically robust joints between alumina substrates using a diffusion bonding process<sup>3</sup>. Diffusion of copper ions into the alumina substrates produces  $\text{CuAlO}_2$  which improves the wettability between the substrate and the joint<sup>4</sup>. The improved wettability increases the strength of the joint as the material is solidified.

In this study, borosilicate glass coupons were joined using a choline chloride-malonic acid DES at temperatures  $<200$  °C. A PV cell-borosilicate glass specimen joined using DES was characterized. A copper-alumina bonding process was attempted to understand the diffusion bonding mechanics.

## **2. EXPERIMENTAL PROCEDURE**

### **2.1. DES PREPARATION**

Deep eutectic solvent (DES) mixtures were prepared by solid state reaction using choline chloride ( $\text{ChCl}$ ;  $>98\%$ , Sigma Aldrich, St. Louis, MO) and malonic acid (MAL;  $99\%$ , Sigma Aldrich, St. Louis, MO). The  $\text{ChCl}$  and MAL powders were dried in an oven at  $50$  °C for a minimum of 24 hours prior to use. The powders were weighed appropriately to prepare DES mixtures containing various molar ratios of  $\text{ChCl}:\text{MAL}$  (0.65, 0.75, 0.85, and 1.00). The molar ratio

values are referred to as the composition factor (CF) of the solvent. The dried powders were combined in a 250 mL Erlenmeyer flask and covered with Parafilm. The combined powders were heated to a temperature of 60 °C and stirred with a magnetic stirrer. For DES-HCl mixtures, 0.1M HCl was added to prepared DES mixtures at a 2:1 volume ratio of DES:HCl.

**2.1.1. Characterization.** The thermal analyses were carried out using a differential thermal analysis/thermogravimetric analysis (DTA/TGA) instrument (Netzsch STA 409 CD) and differential scanning calorimetry (DSC; TA Instruments DSC 2010). For low temperature analysis, DES specimens were sealed in aluminum pans and cooled to <-55 °C using liquid nitrogen. The cooled specimens were heated at a rate of 5 °C/min to a temperature of 50 °C in air. The DES specimens were analyzed using the DTA/TGA for higher temperatures; the specimens were heated at a rate of 5 °C/min to a temperature of 300 °C in either air or argon (UHP, Airgas).

**2.1.2. Dissolution of Metal Salts.** Metal oxide dissolution specimens were prepared using CuO (reagent grade, Sigma Aldrich), Cu<sub>2</sub>O (97%, Sigma Aldrich), Al<sub>2</sub>O<sub>3</sub> (99%, Alfa Aesar), SiO<sub>2</sub> (99.5%, Alfa Aesar), silicic acid (Fisher Scientific) and borosilicate glass powder (BSG). The borosilicate glass powder was prepared by crushing borosilicate glass slides (Thermo Scientific) then sieving to a particle size of <75 µm. Dissolution specimens for metal salts were prepared using CuCl (99%, Alfa Aesar), CuCl<sub>2</sub> (98%, Alfa Aesar), AlCl<sub>3</sub> (98%, Arcos), and AlNO<sub>3</sub>(H<sub>2</sub>O)<sub>9</sub> (99+%, Arcos) in a glovebox back filled with N<sub>2</sub>. An excess of powder (1-2 g powder) was added to 10 mL of DES in an Erlenmeyer



flask (sealed with Parafilm) at a temperature of 60 °C and stirred with a magnetic stirrer for 15 min. The solutions were transferred to a glass test tube and placed in a 50 °C oven for 7 days to allow undissolved oxide powder to settle to the bottom. A 1 mL sample was extracted from the top of the liquid solution and filtered using a 10 mL syringe and 0.45 µm PTFE syringe filter. The filtered specimens were diluted volumetrically with 1 vol% HNO<sub>3</sub> to oxide concentrations between 1 and 100 ppm. The concentrations were analyzed in triplicate using an inductively coupled plasma–optical emission spectrometer (ICP-OES) (Perkin Elmer Avio 200). The reported results were average concentrations multiplied by the dilution multiplier.

## **2.2. JOINED GLASS-PV CELL CHARACTERIZATION**

A sample of joined PV cell-cover glass was cross-sectioned using a low speed saw (Buehler Isomet) and mounted in epoxy. The epoxied specimen was polished with 320, 600, and 1200 grit SiC, then 3 and 1 µm diamond suspension. The join layer was characterized using a micro-Raman spectrometer (Horiba Jobin Yvon LabRAM Aramis, He-Ne laser source, 632.8 nm) and a micro-Fourier transform infrared spectrometer (µ-FTIR, Thermo Nexus 670 FTIR with Thermo Continuum FTIR microscope). The cross-sectioned specimen was sputter coated with gold-palladium (Au-Pd) and imaged using a scanning electron microscope (SEM; Helios Nanolab 600), then analyzed with an energy dispersive spectrometer (EDS; Oxford). Join thickness was determined using ImageJ

software. Ten linear measurements of the join perpendicular to the cover glass edge in the SEM image were averaged.

Another sample of the joined PV cell was separated after heating the specimen on a hot plate to 200 °C and applying a shear force to the join layer. The separated specimen was characterized using a micro-Raman spectrometer and a thin-film x-ray diffractometer (XRD; Philips X'Pert).

### **2.3. JOINING GLASS SLIDES**

Gold Seal borosilicate glass cover slips (22 mm by 22 mm by 0.13 mm) were purchased from Thermo Scientific. The glass cover slips were cleaned with ethanol (99%, Sigma Aldrich) and etched with a 0.1M HCl solution for 20 minutes. Previously prepared DES was heated to 60 °C; a drop of DES was placed in the center of one glass cover slip and another glass cover slip was placed on top. The surface tension of the DES allowed the droplet to spread to the edges of the cover slips.

The samples were placed in a 1" diameter tube furnace that was sealed at both ends. The atmosphere in the furnace was controlled using UHP N<sub>2</sub> and a certified 1% O<sub>2</sub> in N<sub>2</sub> mixture (Airgas). The ratio of N<sub>2</sub> and 1% O<sub>2</sub> was controlled by mass flow controllers (MKS Instruments, 1259C). The furnace was heated to temperatures between 100-150 °C. The samples were held at bonding temperature for a minimum of 20 hours, and then the furnace was shut off and allowed to cool to 60 °C before the specimen was removed.

## 2.4. COPPER-ALUMINA JOINING

An Al<sub>2</sub>O<sub>3</sub> plate (99+%, Coorstek) was machined and cut to dimension (14x14x3 mm) using a surface grinder (600 grit SiC wheel; resin-bonded diamond cutting wheel). The alumina squares were cleaned with ethanol in an ultrasonic bath for 30 mins. Copper foil (0.127 mm thick, annealed, 99.99+%, Alfa Aesar) was oxidized in a furnace at 500 °C for 5 minutes.

The oxidized copper foil was placed between two alumina squares and placed in a sealed tube furnace. The furnace was heated to 1076 °C in N<sub>2</sub>, then 1% O<sub>2</sub> – N<sub>2</sub> was added at a ratio to achieve 0.5 ppm O<sub>2</sub>. The specimen was held at temperature in 0.5 ppm O<sub>2</sub> for 12 hours, and then the furnace was shut off and allowed to cool to room temperature before being removed.

**2.4.1. Characterization.** A shear force was applied to the joined Cu-Al<sub>2</sub>O<sub>3</sub> specimen until the two alumina squares separated. One of the alumina squares was cross-sectioned and mounted in epoxy; the other was mounted in epoxy to expose the join surface. Both samples were imaged using a SEM (15 kV, 1.4 nA) and characterized using EDS (15 kV, 0.43 mA).

## 3. RESULTS AND DISCUSSION

### 3.1. DES CHARACTERIZATION

At low temperatures (<50 °C), the DSC did not measure any distinguishable thermal events for the malonic acid-choline chloride DES (Figure

1). This is in agreement with previous reports that only detected a shift in the baseline at  $-50\text{ }^{\circ}\text{C}$  signifying a change in the heat capacity of the specimen<sup>5</sup>.

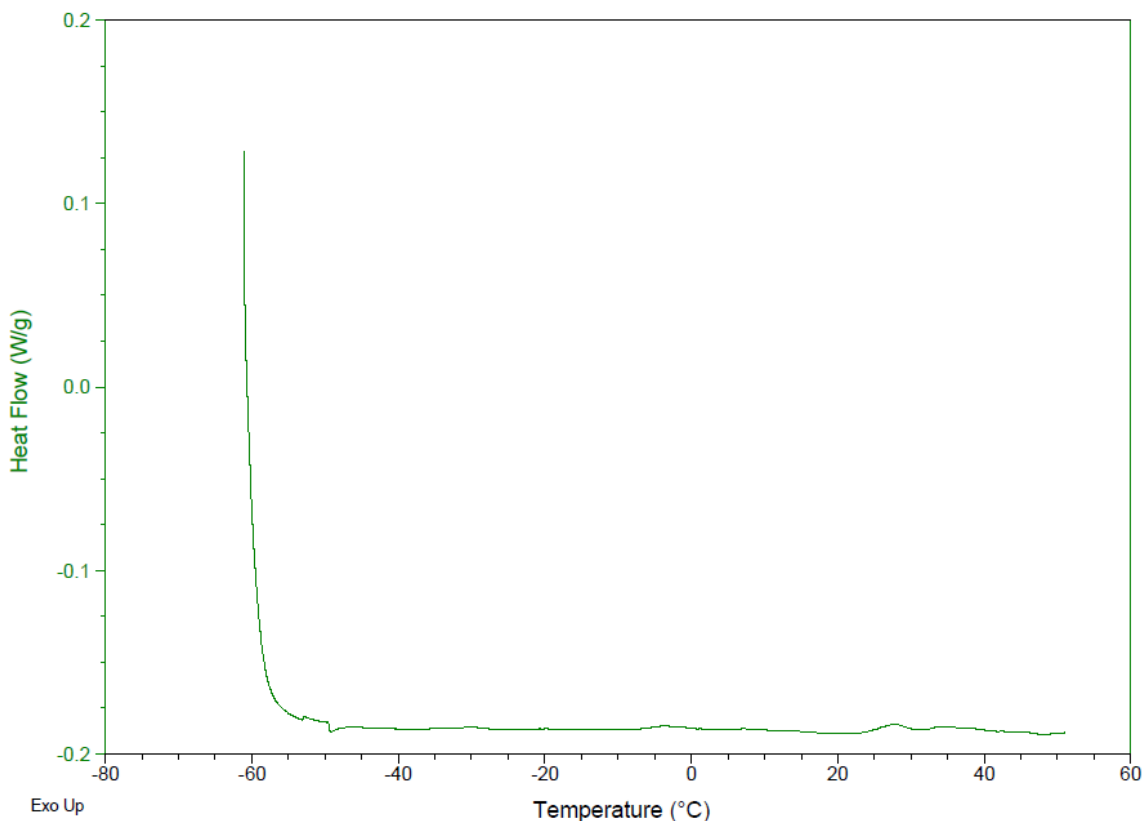


Figure 1. DSC analysis of DES (CF=1) between  $-50\text{ }^{\circ}\text{C}$  to  $50\text{ }^{\circ}\text{C}$

The DTA analysis of the DES detected two distinct endothermic events at  $128\text{ }^{\circ}\text{C}$  and  $262\text{ }^{\circ}\text{C}$ . Comparison to analyses of the individual components shows that these peaks can be attributed to the decomposition of malonic acid ( $156\text{ }^{\circ}\text{C}$ ) and choline chloride ( $285\text{ }^{\circ}\text{C}$ ), respectively (Figure 2). The results indicate that the decomposition of the components shifts to lower temperatures when combined to form the DES, compared to the pure materials heated individually.

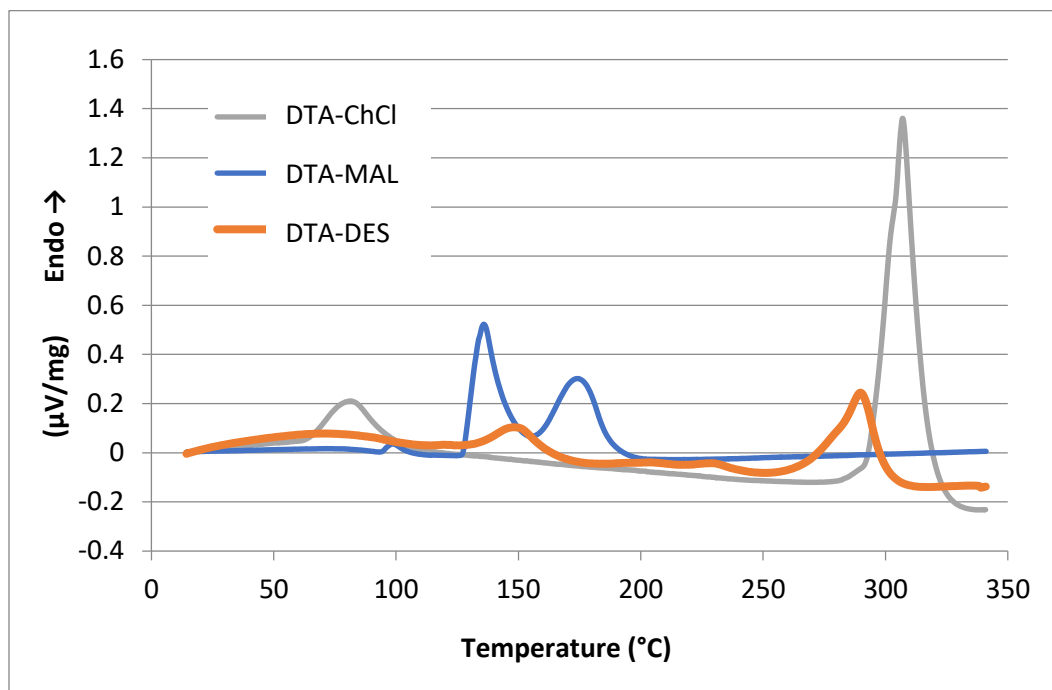


Figure 2. DTA analysis between 20  $^{\circ}\text{C}$  and 340  $^{\circ}\text{C}$  of DES (CF=0.65), MAL, and ChCl under argon

The TGA analysis confirms that the decomposition temperatures decreased after MAL and ChCl were combined to form the DES (Figure 3). The initial decomposition of MAL at 120  $^{\circ}\text{C}$ -150  $^{\circ}\text{C}$  only accounted for 70% of the total mass of MAL in the solvent. This could be related to the non-stoichiometry of the solvent used: the stoichiometric ratio of the eutectic composition is 1 mol ChCl : 1 mol MAL, which suggests that the initial decomposition could be attributed to unreacted MAL.

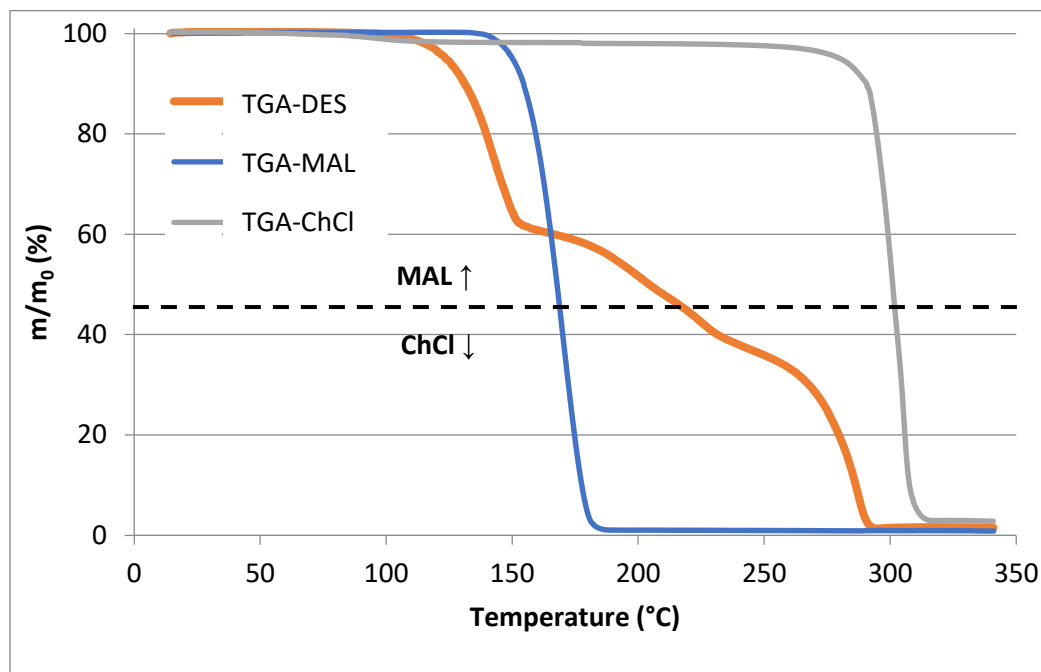


Figure 3. TGA analysis between 20 °C and 340 °C of DES (CF=0.65), MAL, and ChCl under argon. The black dashed line denotes the mass ratio of MAL:ChCl (MAL = 54%, ChCl = 46%).

### 3.2. DISSOLUTION OF METAL SALTS

The concentrations of cations that dissolved increased as the DES composition factor (CF) approached 1 (Table 1). However, the concentrations of the copper ions were maximized at a CF=0.85. The concentration of  $\text{Cu}^{1+}$  ions was 37500 ppm and the concentration of  $\text{Cu}^{2+}$  was 53900 ppm. The concentrations of Si and Al ions were low at all CF values. As CF increased from 0.65 to 1, the  $\text{Si}^{4+}$  concentration increased from 1 ppm to 4 ppm while the  $\text{Al}^{3+}$  concentration increased from 7 ppm to 11 ppm. The addition of the  $\text{Cu}_2\text{O}$ ,  $\text{Al}_2\text{O}_3$ , and  $\text{SiO}_2$  mixture (CAS) showed an overall increase in ion concentrations; at CF=0.65. For example, the  $\text{Si}^{4+}$  concentration increased from 1 ppm when only  $\text{Si}^{4+}$  was present to 13 ppm for the mixture and the  $\text{Al}^{3+}$  concentration increased

from 7 ppm when only  $\text{Al}^{3+}$  was present to 80 ppm for the mixture. Data were not collected for borosilicate glass and CAS at  $\text{CF}=1$ .

Table 1. Concentrations of dissolved metal species (in ppm) in DES mixtures at different CFs

CF	0.65	0.75	0.85	1	
$\text{Cu}^{1+}$	11600 ± 100	28500 ± 2900	37500 ± 300	36500 ± 5200	
$\text{Cu}^{2+}$	12300 ± 100	22100 ± 200	53900 ± 600	51600 ± 5000	
$\text{Al}^{3+}$	7 ± 1	8 ± 1	8 ± 1	11 ± 1	
$\text{Si}^{4+}$	1 ± 1	2 ± 1	2 ± 1	4 ± 1	
BSG ( $\text{Si}^{4+}$ )	1 ± 1	1 ± 1	1 ± 1	X	
CAS	$\text{Cu}^{1+}$	40900 ± 100	40300 ± 1000	41700 ± 900	X
	$\text{Al}^{3+}$	80 ± 1	83 ± 1	76 ± 1	X
	$\text{Si}^{4+}$	13 ± 1	17 ± 1	16 ± 1	X

The addition of aluminum and silicon ions to the  $\text{Cu}_2\text{O}$  had a substantial impact on the copper ion concentrations at lower CF values. At  $\text{CF} = 0.65$ , the  $\text{Cu}^{1+}$  concentration increased from 11550 ppm with no  $\text{Al}^{3+}$  present to 40900 ppm with the addition of  $\text{Al}_2\text{O}_3$  and  $\text{SiO}_2$ . The effect of the CF on the ion concentrations diminished with the aluminum and silicon ions present (Figure 4).

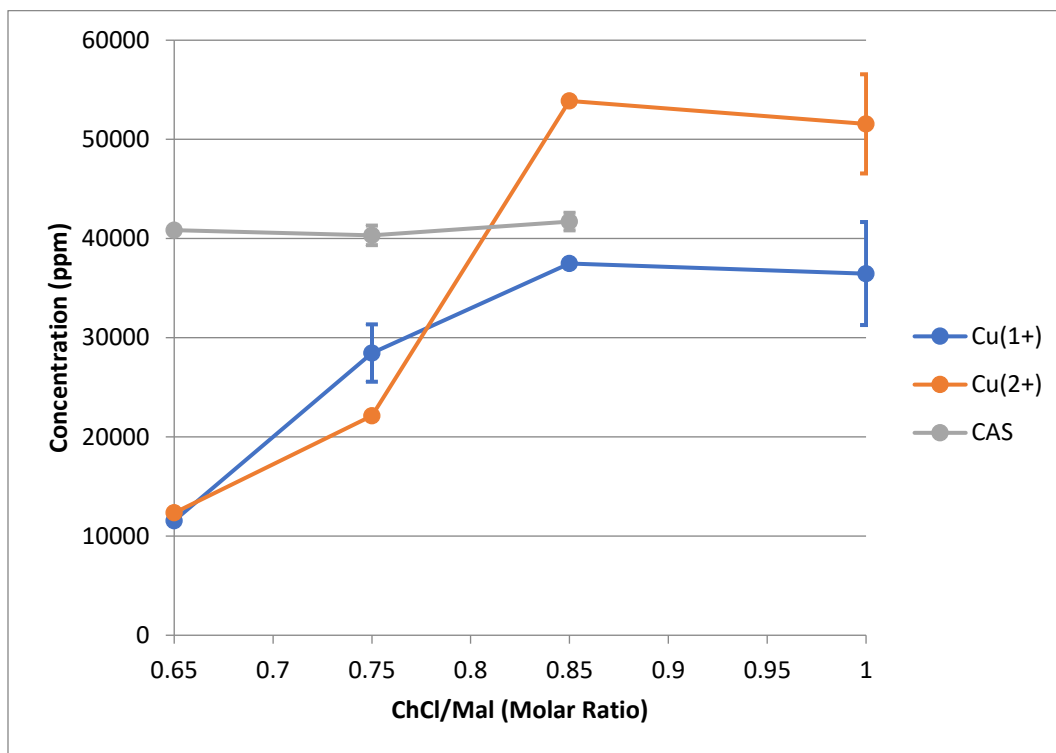


Figure 4. The effect of CF, oxidation state of Cu, and presence of Al and Si ions on Cu ion concentration. Points without error bars have errors smaller than the point size.

The solubility of metal salts was higher than metal oxides for aluminum and silicon, but the Cu ion concentrations that resulted from dissolution of CuCl and CuCl<sub>2</sub> were lower than when the solutions were produced from oxide salts (Table 2). The silicon ion concentration for the silicic acid solution was 79 ppm, about 20 times higher than Si<sup>4+</sup> ion concentrations produced from SiO<sub>2</sub> (4 ppm at CF=1). The addition of other metal salts to the silicic acid did not have a significant effect on the ion concentrations. The aluminum ion concentration was significantly higher when Al(NO<sub>3</sub>)<sub>3</sub>(H<sub>2</sub>O)<sub>9</sub> was dissolved than it was for Al<sub>2</sub>O<sub>3</sub>. The Al<sup>3+</sup> concentration produced by dissolving Al(NO<sub>3</sub>)<sub>3</sub>(H<sub>2</sub>O)<sub>9</sub> was 1200 ppm



compare to 11 ppm for  $\text{Al}_2\text{O}_3$  at  $\text{CF}=1$ . The increase in ionic concentration of metal salts could be attributed to their Lewis acidity. The solvation properties of the DESs stem from the delocalization of the chlorine ion in  $\text{ChCl}$ . The delocalized chloride ion will form metal chloride complexes with molecules that have an affinity to the chloride ion.  $\text{AlCl}_3$ ,  $\text{Al}(\text{NO}_3)_3(\text{H}_2\text{O})_9$  and silicic acid are stronger electron donors than  $\text{Al}_2\text{O}_3$  and  $\text{SiO}_2$ , therefore the delocalized chlorine ion in the DES has a larger effect.

### 3.3. JOINED GLASS-PV CELL CHARACTERIZATION

Five measurements of the join thicknesses from the SEM images were analyzed; the join layer has a thickness of  $18.5 \pm 0.2 \mu\text{m}$  (Figure 5). The relief between the join layer and the surrounding materials was likely due to the polishing process. The join has a lower hardness relative to the PV cell and cover glass, and, therefore, was removed preferentially during polishing, producing relief between the harder outer layers and the softer join layer.

Spot EDS was performed on the join layer at several points: near the PV cell, near the cover glass, and in the center of the join (Figure 6). The atomic concentrations for the EDS spots were similar within a few percentage points indicating that the join composition was uniform, at least within the resolution of EDS. The EDS software detected three elements (disregarding the gold and palladium peaks from the Au-Pd coating applied to the surface of the specimen) within the join: silicon, carbon, and oxygen. The join layer consists of ~25 at% silicon, ~25 at % oxygen, and ~50% carbon (Table 3).

Table 2. Concentrations metal ions (in ppm) produced from metal salts in DES with CF=1

	Base	Silicic Acid		BSG		CAS
Ion	M <sup>+</sup>	M <sup>+</sup>	Si <sup>4+</sup>	M <sup>+</sup>	Si <sup>4+</sup>	M <sup>+</sup>
<b>Cu<sup>1+</sup></b>	33000 ± 1700	40300 ± 200	68 ± 1	37400 ± 200	3 ± 1	36100 ± 100
<b>Cu<sup>2+</sup></b>	14200 ± 100	25100 ± 200	80 ± 1	24700 ± 200	7 ± 1	X
<b>Al<sup>3+</sup></b>	190 ± 10	1570 ± 10	43 ± 1	230 ± 10	0 ± 1	380 ± 10
<b>Al(NO<sub>3</sub>)<sub>3</sub></b>	1190 ± 20	1180 ± 20	53 ± 1	2000 ± 30	5 ± 1	X
<b>Si<sup>4+</sup></b>	79 ± 1	X	X	X	X	49 ± 1

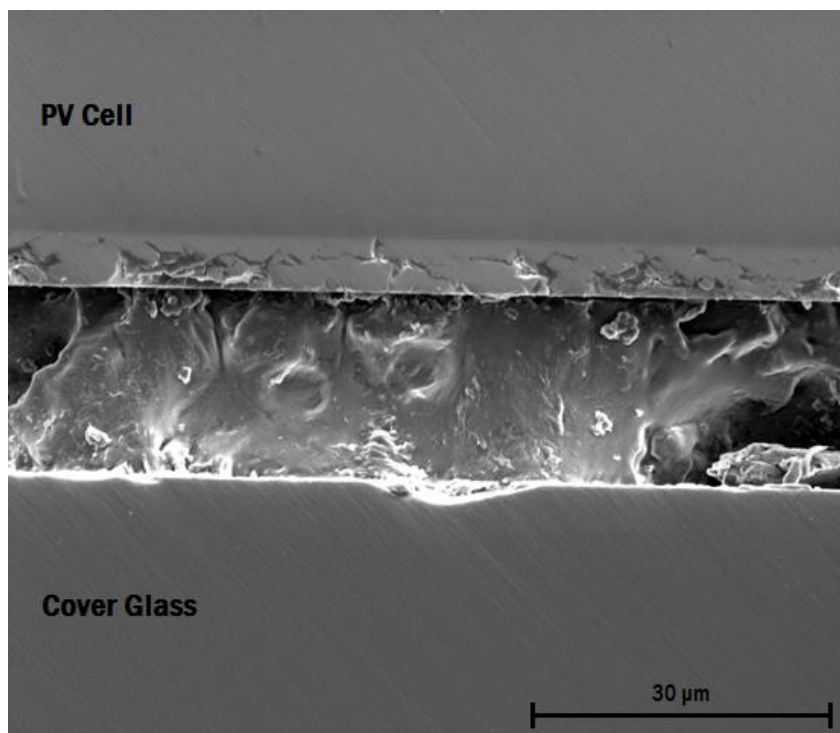


Figure 5. Cross-section of a joined PV cell showing the PV cell (top), join layer (middle), and cover glass (bottom).

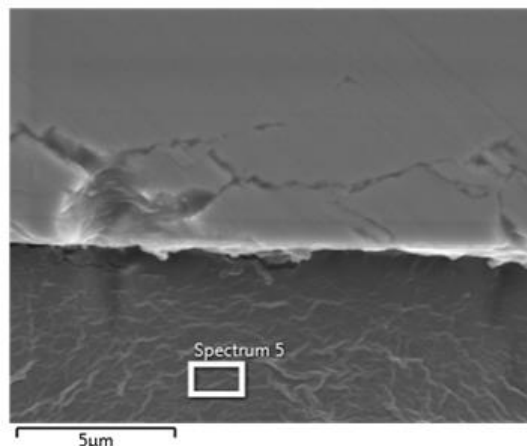


Figure 6. Image showing the location for EDS (spectrum 5) of the join layer taken near the interface with the PV cell

Table 3. Average atomic concentrations measured by spot EDS (Spectrum 5) for the join layer.

Element	Atomic Concentration
Carbon	51 ± 1%
Oxygen	24 ± 3%
Silicon	23 ± 3%

The spectrum obtained from  $\mu$ -FTIR of the cross sectioned PV cell (Figure 7) shows six distinct absorption peaks: 761  $\text{cm}^{-1}$ , 845  $\text{cm}^{-1}$ , 1022  $\text{cm}^{-1}$ , 1100  $\text{cm}^{-1}$ , 1263  $\text{cm}^{-1}$ , and 2333  $\text{cm}^{-1}$ . The 2331  $\text{cm}^{-1}$  peak can be attributed to carbon dioxide in the surrounding atmosphere. Knowing the likely atomic species from the EDS analysis, the remaining five peaks can be attributed to several silicon

species (Table 4):  $761\text{ cm}^{-1}$  and  $845\text{ cm}^{-1}$  are the stretching and rocking vibrational modes of  $\text{Si-CH}_3$ ,  $1022\text{ cm}^{-1}$  and  $1100\text{ cm}^{-1}$  are the stretching vibrational mode of the  $\text{Si-O-Si}$  species, and  $1263\text{ cm}^{-1}$  is the deformation of the  $\text{Si-CH}_3$  species. Analysis of the  $\mu\text{-FTIR}$  spectrum indicates that the join contains both inorganic (e.g.,  $\text{Si-O}$ ) and organic silicon (e.g.,  $\text{Si-C}$ ) bonds. The  $\text{C-H}$  stretching peak ( $2950\text{ cm}^{-1}$ ) is small relative to the silicon peaks and therefore lost in the background noise.

Raman spectroscopy showed two peaks at  $2910\text{ cm}^{-1}$  and  $2970\text{ cm}^{-1}$  which are characteristic of  $\text{C-H}$  bonds (Figure 8). The Raman spectrum supports the findings of the  $\mu\text{-FTIR}$  analysis. The broad peak centered at  $815\text{ cm}^{-1}$  is a fluorescence peak from the interaction between the laser source and the join. The fluorescence peak was significantly larger than the  $\text{C-H}$  peaks, therefore the spectrum was split into two frequency ranges. The second range was acquired for 10x longer than the first. Further analysis of the fluorescence wave number region would require analysis using a different laser wavelength. The Raman spectrum indicates that the join contains an organic component. The  $\text{C-H}$  vibration peaks stem from methyl groups attached to silicon.

The thin film XRD pattern of the separated PV cell suggested that the join layer contained both amorphous and crystalline materials (Figure 9). The pattern contained two distinct peaks at  $38^\circ$  and  $44^\circ$  ( $2\theta$ ) which are characteristic of gold and silver in the (111) and (200) lattice planes, respectively. Since the EDS analysis did not detect gold or silver in the join layer, these peaks are thought to be an artifact of the conductive fingers on the PV cell surface.

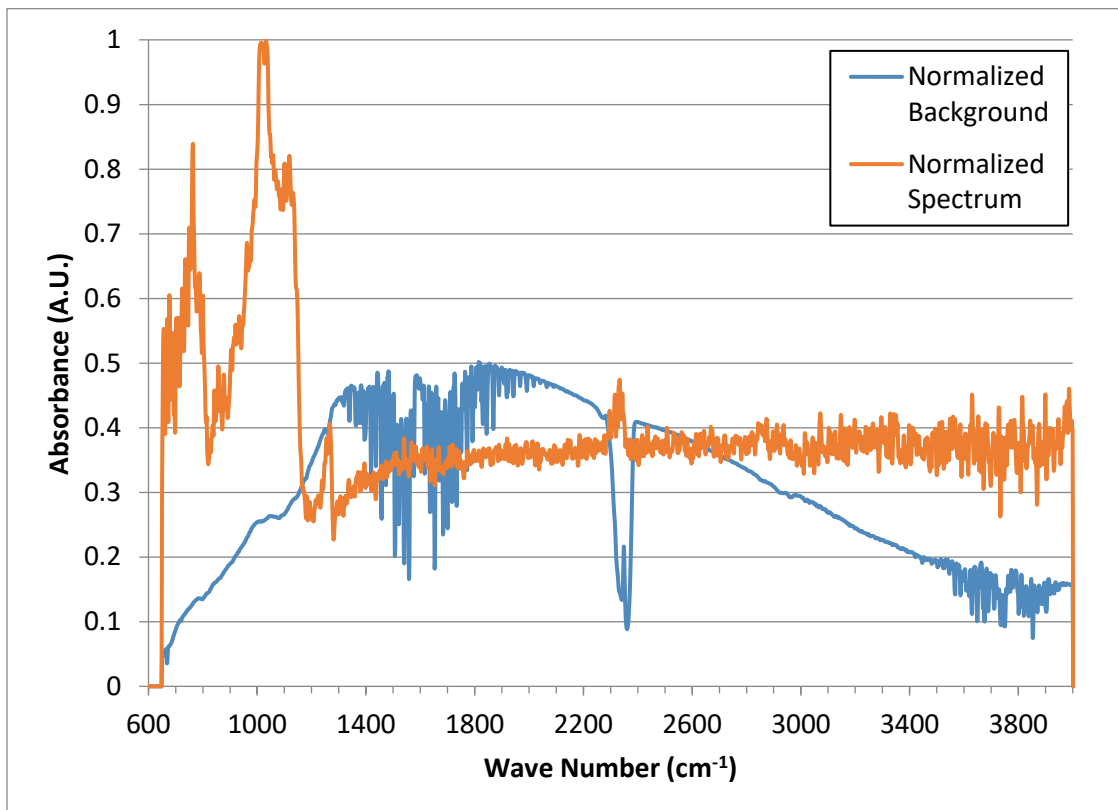


Figure 7.  $\mu$ -FTIR spectra of the joined PV cell specimen and background atmosphere

Table 4. Possible vibrational modes characteristic of the measured  $\mu$ -FTIR peaks<sup>6</sup>.

Measured (cm <sup>-1</sup> )	Reported (cm <sup>-1</sup> )	Vibrational Mode
761	760	Si-(CH <sub>3</sub> ) <sub>3</sub> (Stretching)
845	845	Si-CH <sub>3</sub> (Rocking)
1022	1022	Si-O-Si (Stretching)
1100	1100	Si-O-Si (Stretching)
1263	1262	Si-CH <sub>3</sub> (Deformation)

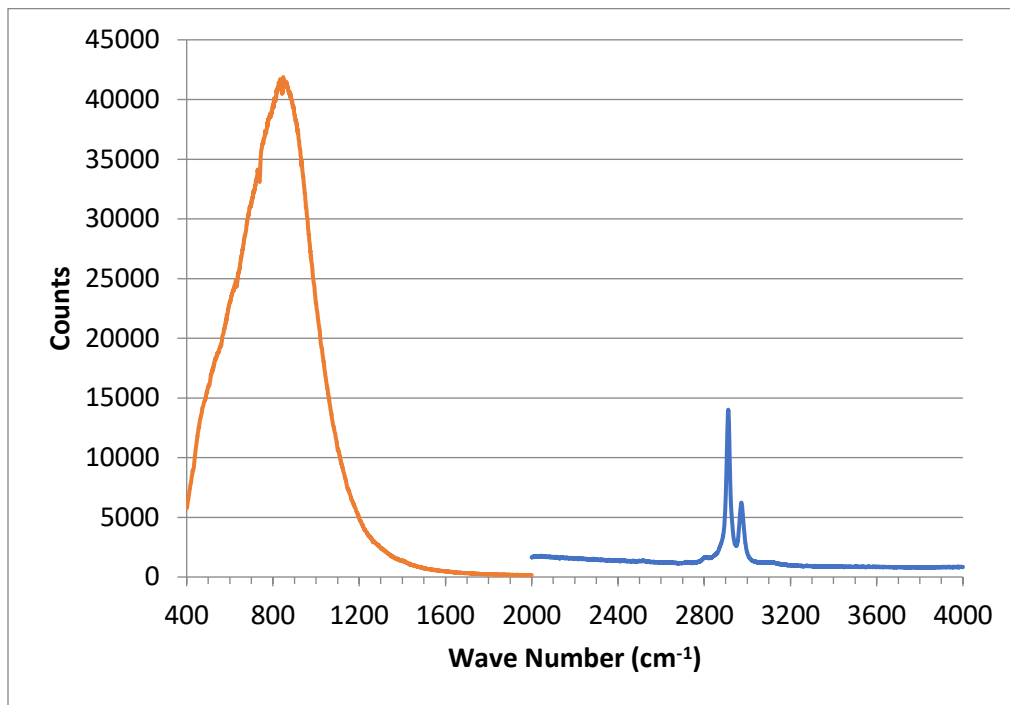


Figure 8. Raman spectra of cross-sectioned joined PV cell using a He-Ne laser source (632.8 nm)

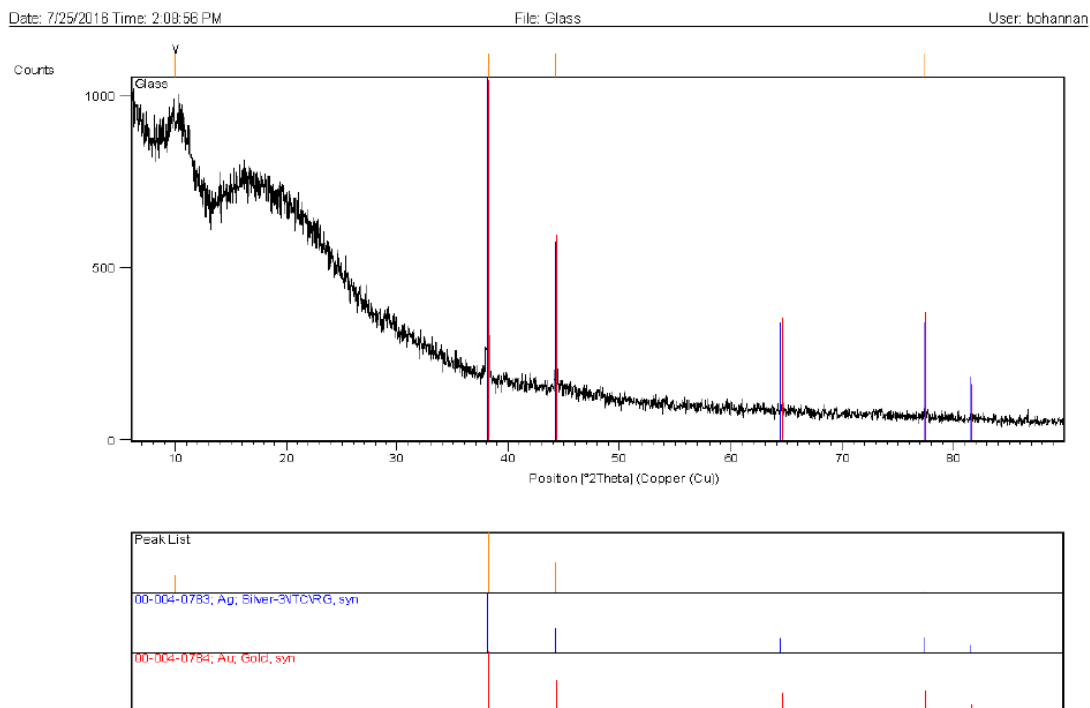


Figure 9. Thin film XRD pattern of the join layer from a separated PV cell-cover glass specimen

After dismissing the conductive finger peaks, the join layer appears to be amorphous. XRD patterns of silicon polymers can vary with extent of crystallization. However, crystallization peaks of silicon polymers are few and disperse, and the pattern will appear largely amorphous<sup>6</sup>. Therefore, the join is an inorganic-organic silicon polymer.

### **3.4. JOINING GLASS SLIDES**

The cover slide specimens appeared to be joined directly after being removed from the furnace after being held isothermally for 20 hours; the join layer was a branching opaque solid. Applying a shear force to the glass cover slides did not immediately separate the cover slides. After approximately one minute out of the furnace, the join material began to convert to liquid around the outer edges of cover glass slides. After liquid formation was noticed, applying a shear force to the cover glass slides resulted in the easy separation of the slides. One of the specimens (CF=0.65, 120 °C, 50 ppm O<sub>2</sub>, 20 hours) was placed in a glovebox under dry UHP N<sub>2</sub> to test the effects of humidity on join stability. Under the dry atmosphere, the specimen remained bonded for several weeks. After removing the specimen from the glovebox, the glass cover slides de-bonded after one day. The DES (CF=0.65) melting temperature is 60 °C, therefore the join remains solid when the glass slide specimens are removed from the furnace at room temperature. However, the DES is hygroscopic and the melting temperature decreases as water content increases. Therefore, the dry nitrogen environment in the furnace causes the DES to solidify when the furnace

temperature decreases below 60 °C, but when the specimen is removed and exposed to ambient atmosphere the DES adsorbs water, reducing the melting temperature below room temperature.

The composition factor of the solvent used in joining did not have a significant effect on the join characteristics. Specimens joined with solvents of CF=1 had a solid join immediately after being removed from the furnace, but began to form a liquid on the outer edges within 1 minute. The specimen held at 120 °C in an atmosphere with 50 ppm O<sub>2</sub> for 144 hours had similar characteristics to a specimen held for 20 hours under the same condition. Both de-bonded after 1 minute. Therefore, the duration of the heat treatment does not affect the success of the join. The joins remained transparent when joining was performed below 150 °C and at pO<sub>2</sub> values less than 150 ppm. Higher temperatures or pO<sub>2</sub> values caused the joins to turn brown. TGA data shows the initial decomposition temperature of the DES was 120 °C (Figure 3), corresponding to the decomposition of the MAL component of the DES. At low oxygen content, MAL experiences tautomerization at its decomposition temperature forming two gaseous species, carbon dioxide and acetic acid. Currently there are no studies on the decomposition of the MAL/ChCl DES, but the presence of ChCl clearly affects the decomposition of the MAL (Figures 2 and 3).

The addition of 0.1M HCl to the DES did not have a significant effect on the join success, but the join remained colorless.



Specimens joined with metal oxides added to the DES remained joined for less than a minute after being removed from the furnace. Joins produced from DES mixtures that contained  $\text{Al}_2\text{O}_3$  and  $\text{SiO}_2$  remained transparent, but the DES with  $\text{Cu}_2\text{O}$  added was green. The DES- $\text{Cu}_2\text{O}$  mixture was green previous to the joining process. The addition of metal oxide salts did not improve the joining characteristics.

### 3.5. JOINING $\text{Al}_2\text{O}_3$ WITH CU INTERLAYERS

The copper foil was oxidized prior to joining based on results from a previous study<sup>4</sup>. The oxygen content of the copper has a significant effect on its wetting of alumina. Oxygen content below 0.03 at% in the  $\text{Cu}_{(\text{ss})}$  will increase the wetting angle, producing a poor join. The optimal oxygen content in  $\text{Cu}_{(\text{ss})}$  is between 0.03 at% and 1.7 at%. Previous studies pre-oxidized the copper foil at 1000 °C for 4 minutes<sup>7</sup>. However, a study observing the strength of  $\text{Cu-Al}_2\text{O}_3$  bonds found that the presence of  $\text{Cu}_2\text{O}$  particles decreases the strength<sup>8</sup>.  $\text{Cu}_2\text{O}$  preferentially forms when oxidizing copper at 1000 °C in air. The strength of the  $\text{Cu-Al}_2\text{O}_3$  bond will increase when a thin (300-500 nm)  $\text{CuO}$  film is formed on the surface of the copper foil. In air,  $\text{CuO}$  will preferentially form on the copper foil at lower temperatures (<1000 °C) than  $\text{Cu}_2\text{O}$ .

In the first experiment, copper foil was initially centered between two alumina pieces (Figure 10), but after the thermal treatment the alumina pieces shifted and some of the copper formed a bead outside of the join region (Figure 11). The formation of the bead indicates that the wetting angle between the

copper and alumina was too large for stable join formation. In future  $\text{Al}_2\text{O}_3$  joining experiments, the oxygen content of the foil will be increased by increasing the pre-oxidation time, controlling the oxygen partial pressure during the pre-oxidization process, or increasing the oxygen partial pressure during the bonding process.

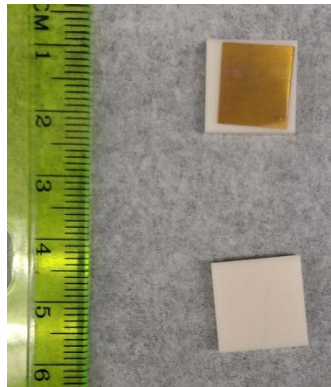


Figure 10. Image of oxidized copper and alumina pieces before joining

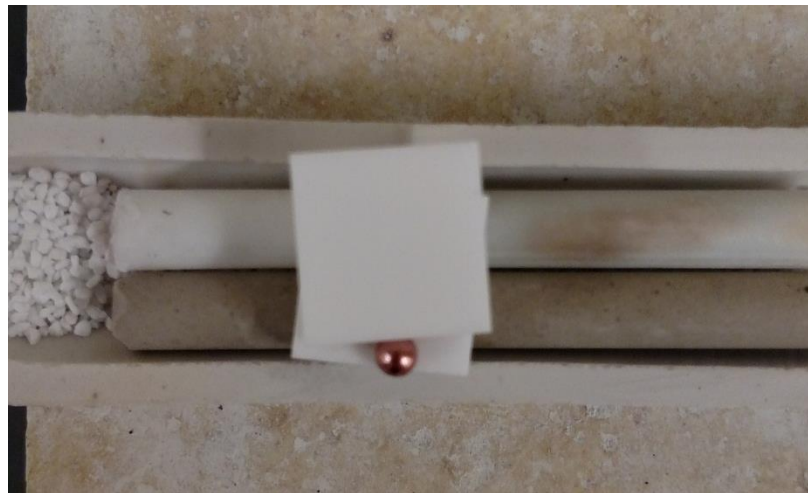


Figure 11. Image of  $\text{Al}_2\text{O}_3$  specimen after heating.

After separating the alumina pieces, a region of discoloration was apparent on the alumina pieces. The discolored region corresponded to where the copper foil was in contact with the alumina pieces (Figure 12).

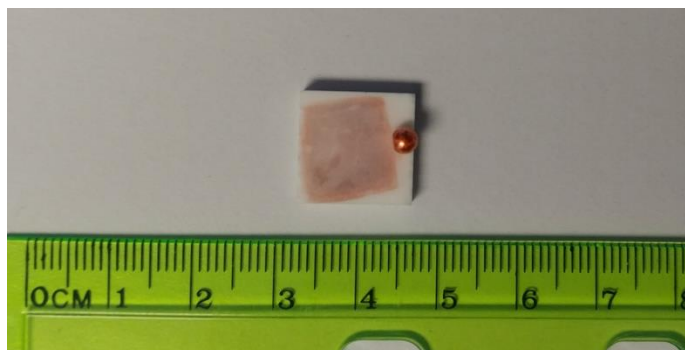


Figure 12. Image of separated  $\text{Al}_2\text{O}_3$  after heating illustrating the region of interaction where copper foil and alumina were in contact

A cross-sectioned joined Cu- $\text{Al}_2\text{O}_3$  specimen was examined using SEM. The image focused on the region where the copper was in contact with the alumina piece during heating. The SEM image did not show a significant difference in microstructure of the metal contact region compared to the bulk alumina piece. An EDS map of the interface cross section indicated that no substantial infiltration of copper occurred (Figure 13).

The EDS maps of the alumina surface that contacted the copper showed that a few, isolated copper-rich regions (blue spots in Figure 14) were observed. However, EDS did not indicate that Al or O were present in significant quantities, which presumably indicated that no  $\text{CuAlO}_2$  formed. The isolated copper regions

indicate that the parameters used during the joining process were not suitable for stable joint formation.

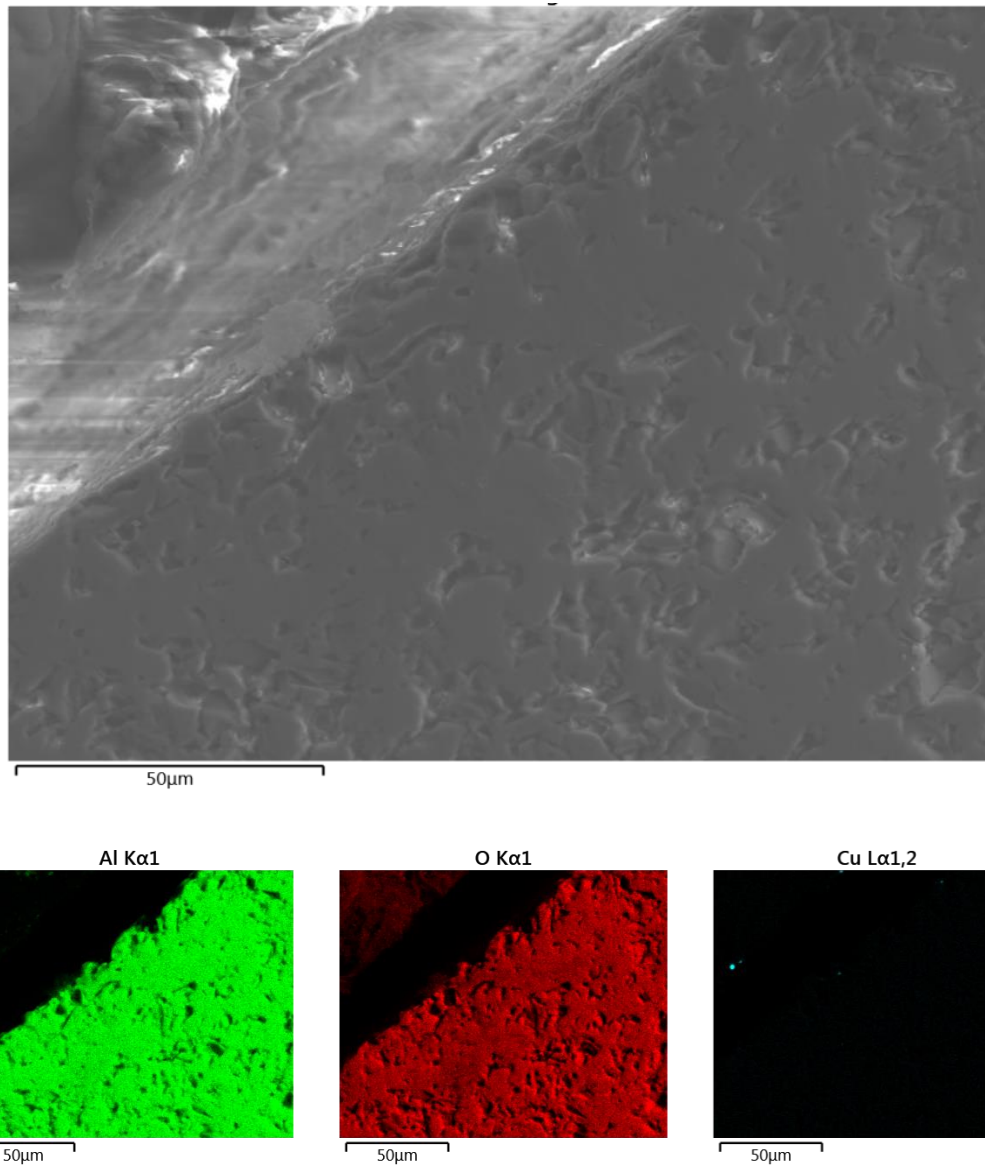


Figure 13. SEM image and EDS maps of cross-sectioned of separated Cu-Al<sub>2</sub>O<sub>3</sub> specimen

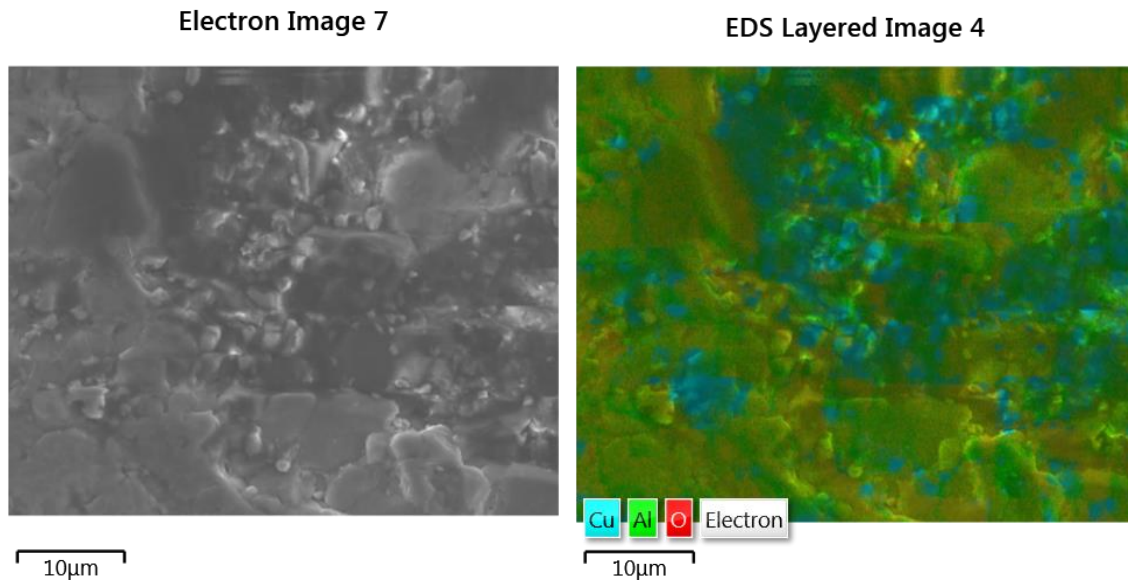


Figure 14. SEM image and the composite EDS map of the surface where the copper foil was in contact with the alumina.

#### 4.CONCLUSIONS

In this study the joining of ceramic materials at low temperatures was investigated. To investigate the viability of choline chloride-malonic acid DES as joining medium for borosilicate glasses, the thermal characteristics and the dissolution of metal salts in DES were studied. Joining of borosilicate glass was attempted using DES at temperatures between 100 °C to 150 °C and various partial pressures of oxygen. A photovoltaic cell specimen joined to borosilicate glass was characterized using SEM, EDS, thin film XRD,  $\mu$ -FTIR and Raman spectroscopy. Finally, joining of alumina pieces was attempted using copper foil and a diffusion bonding technique. The joined alumina specimen was characterized using SEM and EDS.

The solubility of silica in DES was maximized at a composition factor of 1, but the solubility of silica was inadequate to produce an inorganic join with borosilicate glass. Additions of other oxides or metal salts such as  $\text{Al}_2\text{O}_3$  or silicic acid increase the solubility of silica, but not significantly.

Various characterization techniques showed that a PV cell join consisted of an amorphous solid that contained silicon with inorganic (e.g., Si-O) and organic (e.g., Si-C) bonds. Elemental analysis did not detect any additional elements beyond silicon, oxygen and carbon in those joins.

Joining experiments with DES and borosilicate glasses were conducted at various temperatures and  $p\text{O}_2$  values. Under all conditions, a hygroscopic join layer formed. The joins were not stable in the ambient atmosphere due to reaction with water vapor, so further characterization was not performed.

The Cu- $\text{Al}_2\text{O}_3$  joining experiment did not produce a successful join; however, there was a small amount of metal retained between the alumina pieces. Based on poor wetting of the alumina by molten copper, the oxygen content of the copper foil was concluded to be too low to produce a sufficiently low wetting angle to achieve successful joining. No evidence was found to conclude that  $\text{CuAlO}_2$  formed at the interface between the copper and alumina.

## REFERENCES

- 1 A.P. Abbott, G. Capper, D.L. Davies, H.L. Munro, R.K. Rasheed, and V. Tambyrajah, "Preparation of Novel, Moisture-Stable, Lewis-Acidic Ionic Liquids Containing Quaternary Ammonium Salts With Functional Side Chains," *Chem. Commun.*, [19] 2010–2011 (2001).
- 2 A.P. Abbott, G. Capper, D.L. Davies, K.J. McKenzie, and S.U. Obi, "Solubility of Metal Oxides in Deep Eutectic Solvents Based on Choline Chloride," *J. Chem. Eng. Data*, (2006).
- 3 C.W. Seager, K. Kokini, K. Trumble, and M.J.M. Krane, "The Influence of CuAlO<sub>2</sub> on the Strength of Eutectically Bonded Cu/Al<sub>2</sub>O<sub>3</sub> Interfaces," *Scr. Mater.*, **46** [5] 395–400 (2002).
- 4 M. Diemer, A. Neubrand, and K.P. Trumble, "Wettability in the Copper – Oxygen – Alumina System," *J. Am. Ceram. Soc.*, **82** 2825–2832 (1999).
- 5 H.G. Morrison, C.C. Sun, and S. Neervannan, "Characterization of Thermal Behavior of Deep Eutectic Solvents and Their Potential as Drug Solubilization Vehicles," *Int. J. Pharm.*, **378** [1–2] 136–139 (2009).
- 6 A.L. Smith, *The Analytical Chemistry of Silicones*. John Wiley & Sons, Inc., New York, NY, 1991.
- 7 Y. Yoshino, "Role of Oxygen in Bonding Copper to Alumina," *J. Am. Ceram. Soc.*, **72** [8] 1322–1327 (1989).
- 8 H. Ghasemi, A. H. Kokabi, M. A. Faghihi Sani, and Z. Riazi, "Roles of Preoxidation, Cu<sub>2</sub>O Particles, and Interface Pores on the Strength of Eutectically Bonded Cu-Al<sub>2</sub>O<sub>3</sub>," *Mater. Des.*, **30** [4] 1098–1102 (2009).

## **II. LOW TEMPERATURE JOINING OF BOROSILICATE GLASS UTILIZING CHOLINE HYDROXIDE**

**ERIC MUSKOVIN AND WILLIAM FAHRENHOLTZ**

**MISSOURI UNIVERSITY OF SCIENCE AND TECHNOLOGY**

### **ABSTRACT**

Choline hydroxide (ChOH) was used to join borosilicate glass at temperatures below 200 °C. Silica has high solubility in ChOH, which can be exploited to form organic-inorganic hybrid joins with high optical transmission. Thermal analyses showed that alcohol condensation reactions occurred at temperatures as low as 67 °C. Solidification of the join occurred at 67 °C in air over a period of 20 hours. Optical transmission spectroscopy showed that the join exhibited >80% optical transmission at wavelengths between 350-1100 nm. However, the decomposition of the ChOH caused optical characteristics to deteriorate when held at temperatures greater than 70 °C.

### **1. INTRODUCTION**

Sol-gel processing techniques have been studied to produce optical-quality joins with inorganic substrates for solar cell applications. Sol-gel is particularly attractive for joining semiconductor substrates because of its ability to produce inorganic and optically transparent materials at low temperatures<sup>1</sup>. For



solar cell applications, volatile species including solvents or products of hydrolysis and condensation reactions could get trapped between impermeable substrates, which would affect adhesion and optical properties. Evaporation of volatiles during the drying process could also cause the gel to shrink resulting in warping or cracking of the join.

Organic-Inorganic (O-I) hybrid materials materials contain inorganic and organic components. The mechanical and optical properties of O-I materials can be altered by varying the relative amounts of inorganic and organic components<sup>2,3</sup>. Ormosils are O-I materials that are based on organically-modified silica networks. The addition of silyl groups (Si-C) increases the elasticity and decreases the refractive index compared to nominally pure silica.

Hexamethyldisilazane (HMDS) is a common silylating agent used to produce O-I hybrid materials for applications such as superhydrophobic antireflective coatings<sup>2,4,5</sup>. Sol-gel processing techniques have been used to produce ormosils through the additions of alkoxysilanes as an inorganic component and HMDS as the organic component<sup>6-9</sup>.

Quaternary ammonium hydroxides (QAHs) are strong organic bases that exhibit high silica solubility<sup>10</sup>. Silica anions in QAH solutions form cage-like structures based on structural units such as  $\text{Si}_6\text{O}_{15}^{6-}$ ,  $\text{Si}_8\text{O}_{20}^{8-}$ , and  $\text{Si}_{10}\text{O}_{25}^{10-}$ . In solutions containing 2-hydroxyethyl trimethylammonium hydroxide or choline hydroxide (ChOH), silica polymerizes to form a double ring cage structure known as a cubic octasilicate anion ( $\text{Si}_8\text{O}_{20}^{8-}$ ). The cubic octasilicate anion consists of

two four-membered rings of silica tetrahedra that form a cube with oxygen ions at the corners<sup>11</sup>.

In this study, borosilicate glass coupons were joined using a low temperature sol-gel technique. Fumed silica was dissolved in a ChOH-methanol solution to form cubic octasilicate anions in solution. Alkoxysilanes were added to cross-link the cubic octasilicate molecules and form a 3-dimensional silica network. HMDS was added as a network modifying agent to reduce drying stresses in the final join.

## **2. EXPERIMENTAL PROCEDURE**

### **2.1. LIQUID PRECURSOR PREPARATION**

Liquid precursors were prepared using choline hydroxide in methanol solution (ChOH; 45 wt% choline hydroxide Sigma Aldrich, St. Louis, MO), fumed silica (7 nm, Aldrich Chemical Co., St. Louis, MO), tetramethoxysilane (TMOS; 99%, Aldrich Chemical Co., Milwaukee, WI), tetraethoxysilane (TEOS; reagent grade, Fisher Scientific, Fair Lawn, NJ), and hexamethyldisilazane (HMDS; reagent grade, >99%, Aldrich Chemical Co., St. Louis, MO). The ChOH solution was added to a 250 mL Erlenmeyer flask and covered with a rubber stopper. Fumed silica was added gradually to the ChOH at room temperature and stirred with a magnetic stirrer until a 25 wt% silica solution was produced. The ChOH-silica solution was placed in a 100 mL Teflon beaker uncovered and stirred with a magnetic stirrer. TMOS or TEOS and HMDS were added to produce liquid

precursors with various molar ratios (Table 1). The liquid precursors were stirred continuously for two hours at room temperature to evaporate excess methanol and ammonia.

Table 1. Molar ratios of components in liquid precursors

Precursor	Dissolved Silica	TMOS	TEOS	HMDS
CM	4	1	0	0
CE	4	0	1	0
CMH	6	1	0	1
CEH	6	0	1	1

## 2.2. BONDING

Gold Seal borosilicate glass microscope cover slides (22 mm by 22 mm by 0.13 mm, Thermofisher, St. Louis, MO) were placed in concentrated HCl (ACS grade, 37% HCl, Fisher Science, Nazareth, PA) for 20 hours, then rinsed with deionized water and dried with laboratory wipers. A ~7 mm diameter drop of one of the liquid precursors was placed in the center of one of the glass coupons and sandwiched by another glass coupon. Slight pressure was applied to reduce joint thickness so that excess liquid precursor squeezed out from between the glass coupons.

The sandwiched specimens were placed in a 1" diameter tube furnace that was sealed at both ends. The atmosphere in the furnace was controlled

using a continuous flow of an UHP argon gas (Airgas) for some of the specimens (designated with "Ar"). For the other specimens, the furnace atmosphere was stagnant air. The furnace was heated to temperatures between 65-150 °C. The samples were held at bonding temperature for a minimum of 20 hours, and then the furnace was shut off and allowed to cool to 60°C before specimens were removed. The process was repeated to produce bonded specimens for each of the precursor compositions.

### **2.3. THERMAL STABILITY**

A furnace was heated to a temperature between 70-150 °C in air. Three bonded CMH specimens were placed on an aluminum pan in the furnace for an hour at temperature. After one hour, the specimens were removed from the furnace and cooled to room temperature on a fire clay refractory brick.

### **2.4. CHARACTERIZATION**

Thermal analyses were carried out using differential scanning calorimetry and thermogravimetric analysis (DSC/TGA; TA instruments, SDT Q600). Solid CMH specimens were produced by placing a ~7 mm diameter drop of liquid CMH onto a borosilicate glass coupon and holding the specimen at 67 °C in air for 20 hours. Liquid precursors and solid CMH specimens were heated to 300 °C at a ramp rate of 5 °C/min in air and under 100 mL/min flow of nitrogen (UHP, Airgas). The onset temperatures were determined by the intersection of lines tangent to the slopes of the DSC before and after the onset of the thermal

events. For peaks with indeterminable onset temperatures, the peak temperatures are presented.

The bonded specimens and thermal stability specimens were analyzed using a UV-Vis spectrometer (Thermo Scientific, Genesys 10uv); two non-bonded slides were also analyzed. The UV-Vis analyses were performed in triplicate, a single spectrum was selected to be representative of the specimen.

Liquid precursors and solid specimens were characterized using a micro-Raman spectrometer (Horiba Jobin Yvon LabRAM Aramis, He-Ne laser source, 632.8 nm). The spectrometer was calibrated with a silicon standard.

### 3. RESULTS AND DISCUSSION

#### 3.1. DSC/TGA CHARACTERIZATION

**3.1.1. Liquid Precursors.** Thermal gravimetric analysis (Figure 1) showed that the mass of the ChOH-silica solution decreased by approximately 10% when heated to 90°C. This was the result of methanol evaporation. The DSC analysis detected three large endothermic transitions. The onset temperature for the first endothermic transition was approximately 90 °C and the peak from the second transition overlapped with the first. The onset of the second endothermic transition was approximately 130 °C. Both of the first two endothermic transitions can be attributed to the decomposition of the choline hydroxide identified by the fishy odor that was expelled from the DSC/TGA exhaust. Choline hydroxide decomposed into trimethylamine and vinyl alcohol<sup>12</sup>. Trimethylamine gas has a

characteristic strong fishy odor even in low concentrations. The mass of the solution decreased by 35% from 92 wt% at 90 °C to 57 wt% at 130 °C, which is consistent with the amount of ChOH relative to the total mass of the solution (34%). The third endothermic transition has an onset temperature of 170 °C and is attributed to the remaining water condensation reactions between molecular silica species. At temperatures above 250 °C, the TGA analysis showed that 29 wt% of the original solution remained. Considering that approximately 25 wt% of the starting solution was silica, the solid produced above 250 °C was largely composed of the silica. The difference in weight could be attributed to solvent evaporation before the analysis or remaining organics trapped in the specimen.

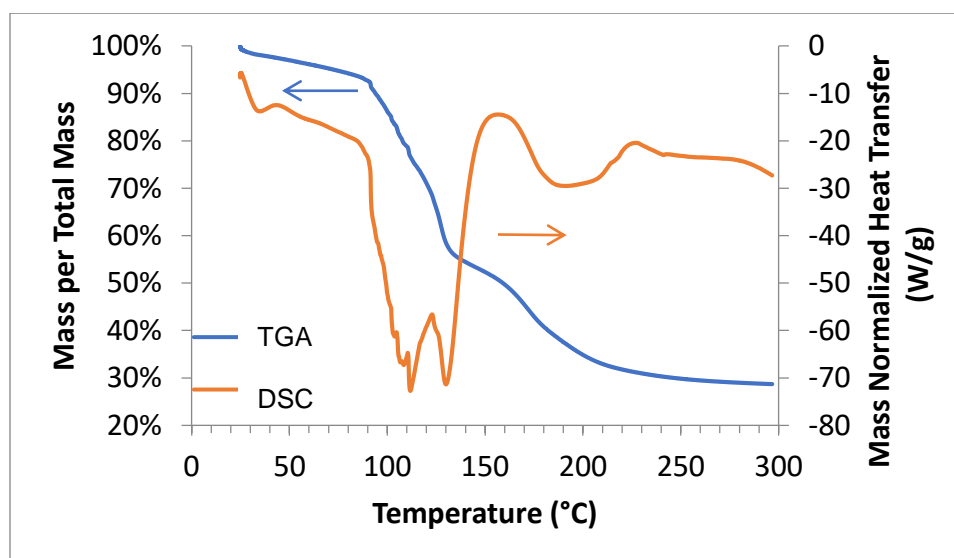


Figure 1. DSC/TGA of choline hydroxide-silica solution in air

The TGA analysis of the CM liquid precursor was similar to the ChOH-Silica solution (Figure 2). At 90 °C, the mass decreased more rapidly like that of

the ChOH-Silica solution. The mass loss rate increased from  $-0.14\%/^{\circ}\text{C}$  under  $90^{\circ}\text{C}$  to  $-3.0\%/^{\circ}\text{C}$  above  $90^{\circ}\text{C}$ . However, the DSC analysis showed a smaller endothermic peak in the CM liquid precursor than the ChOH-Silica solution. The change in mass normalized heat transfer was  $8.8\text{ W/g}$  for CM liquid and  $52.2\text{ W/g}$  for ChOH-Silica solution. The CM liquid precursor DSC analysis also contained the ChOH decomposition and water condensation endothermic peaks. Above  $250^{\circ}\text{C}$ , the CM precursor retained  $\sim 33\text{ wt\%}$  of the original mass, which indicated that the addition of TMOS increased the silica concentration in the solution and the overall silica yield in the final solid product.

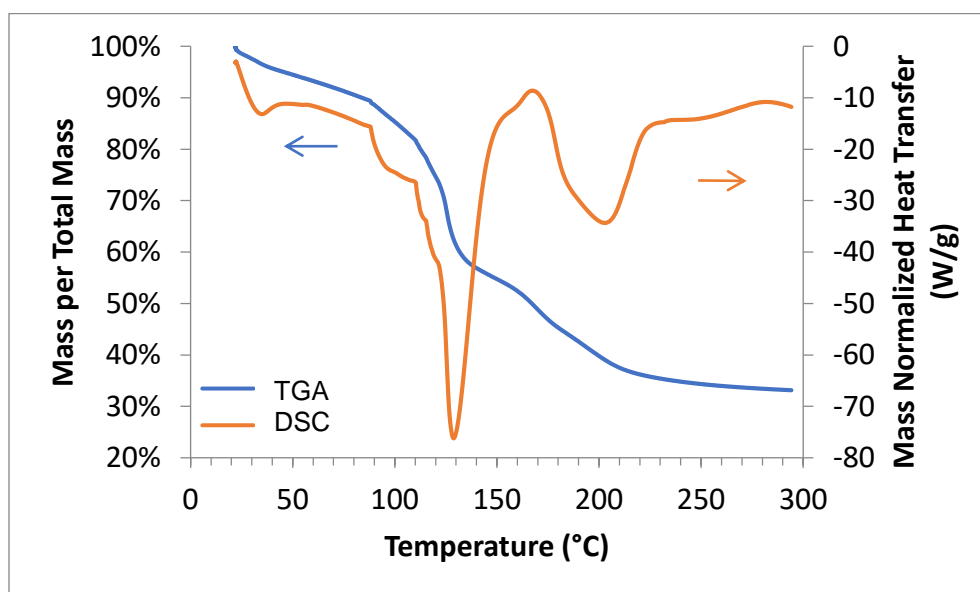


Figure 2. DSC/TGA data of CM liquid precursor

The addition of HMDS changed the TGA and DSC results at temperatures below  $90^{\circ}\text{C}$  (Figure 3). Similar to the CM liquid precursor and the ChOH-silica solution DSC analyses, the CMH liquid precursor analysis contained the

endothermic peaks related to the decomposition of ChOH and the silica condensation reaction. However, a small endothermic peak appeared at 67 °C in the CMH analysis that was not present in the other analyses. The peak was not likely due to ChOH decomposition as the trimethylamine smell was not apparent until ~90 °C, which indicates that the concentration is below its detection limit (0.21 ppb). The TGA analysis indicated a more prominent decrease in mass below 90 °C than CM liquid precursor and ChOH-silica solution. This was likely due to the evaporation of ammonia, which is a byproduct from the HMDS condensation reaction in addition to methanol evaporation from the original solution. The smell of ammonia was apparent at the start of the thermal analysis (<46.8 ppm). The amount of ammonia in the liquid precursor was relatively small as most of the ammonia was evaporated during the preparation of the precursor.

Comparing the DSC analyses of CE and CM, the analyses are nearly identical (Figure 4). The onset temperature of the first endothermic transition was increased slightly in the CE compared to the CM liquid, but not significantly.

The TGA analysis of the CE liquid precursor showed a larger decrease in mass than CM liquid below 90 °C; CE retained ~80% of its original mass at 90 °C compared to ~90% for CM at the same temperature (Figure 5). Above 90 °C, the TGA analyses of CE and CM were similar, but the difference between the CE and CM mass percentage decreases from 10% to 3% at 300 °C.



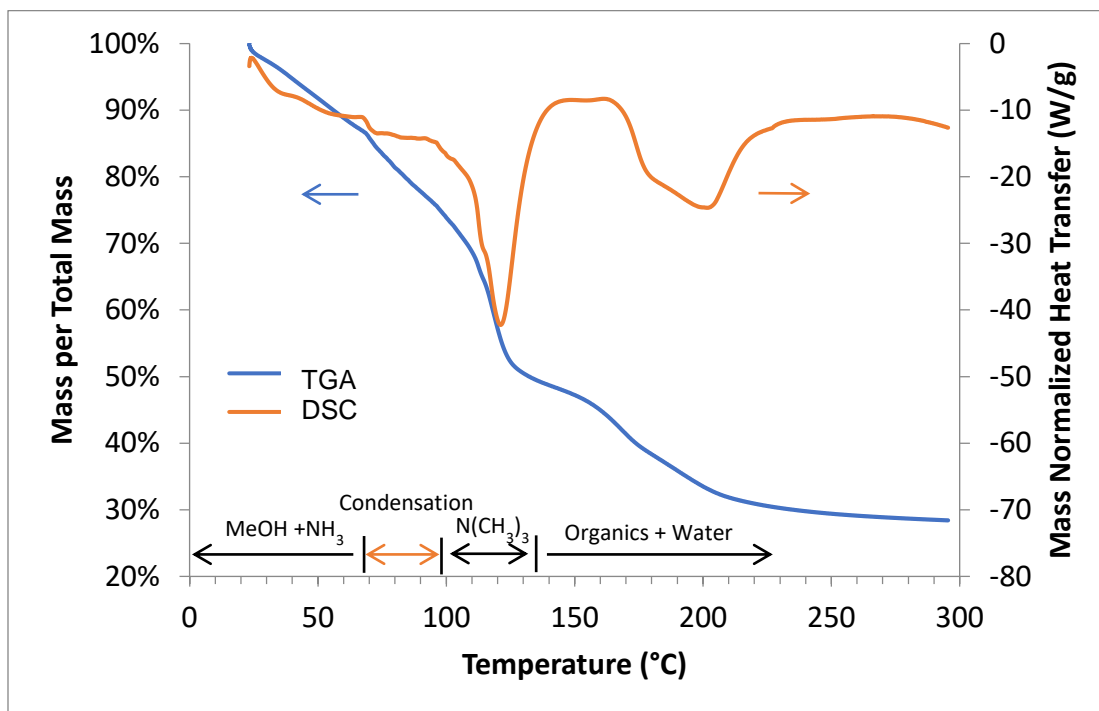


Figure 3. DSC/TGA analyses of CMH liquid precursor.

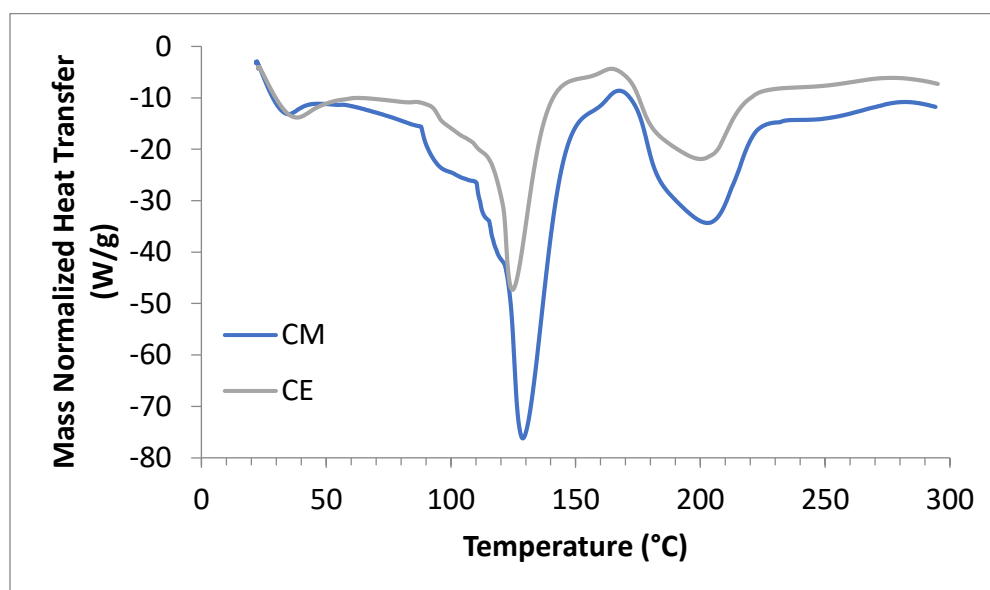


Figure 4. Comparison of DSC analyses for CM and CE precursors.

The difference in mass change of CM and CE at 300 °C was likely due to difference in silica yield between the TEOS and TMOS in the corresponding initial liquid precursor. TEOS and TMOS produce the same number of moles of silica in condensation reactions. However, at low temperatures, hydrolysis of TEOS produces ethanol while TMOS will produce lighter methanol resulting in less mass loss associated with the reaction products for TMOS hydrolysis and condensation. At 80 °C, the ethanol (b.p.= 78 °C) and methanol (b.p. = 67 °C) were completely evaporated.

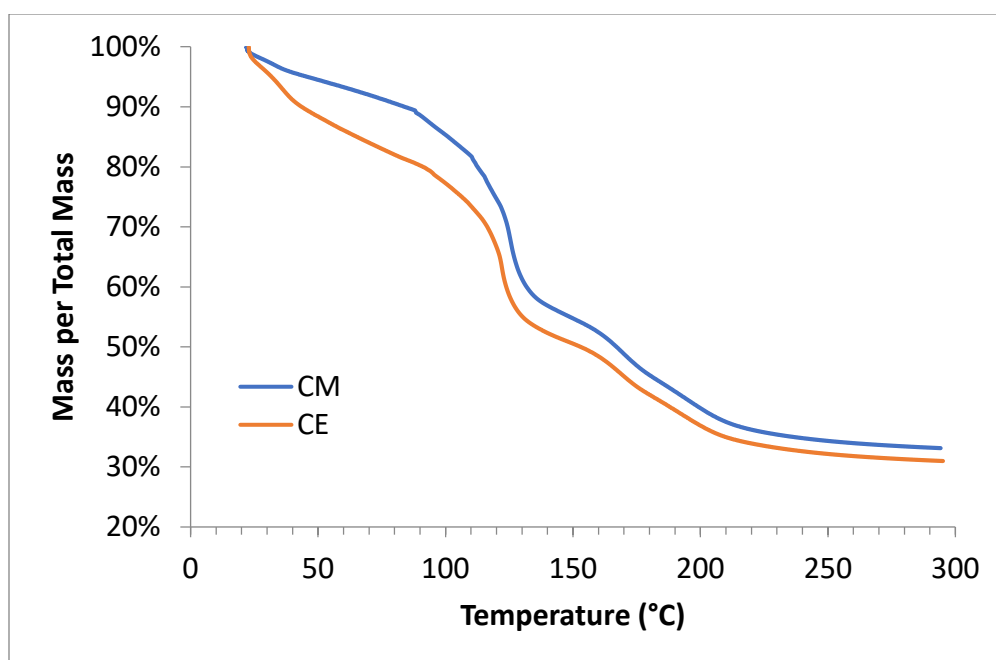


Figure 5. TGA analyses of CM and CE precursors

The DSC analysis of the liquid precursor containing TEOS and HMDS (CEH) had a fourth endothermic transition at 80 °C (onset) that was not present in the CMH DSC analysis (Figure 6). The endothermic peak was attributed to the

evaporation of ethanol produced from alcohol condensation. Similar to the CMH DSC analysis, CEH had endothermic peaks identified from methanol evaporation (67 °C) and decomposition of  $\text{CH}_3\text{OH}$  (128 °C peak). At temperatures above 170 °C, it became more apparent that the endothermic peak previously attributed to the water condensation reaction was actually two convoluted endothermic peaks. In the case of CEH, the first peak at 170 °C onset was more prominent than the peak at higher temperatures, while in the previous liquid precursors it was the opposite. The water condensation peak should be similar for all liquid precursors as they all contain the same amount of hydrolyzed silica species. Therefore, it was likely that the second peak was due to the water condensation reaction. Although the peak at 170 °C could not be easily identified in the CM and CMH liquids, the difference in peak intensity between the CE and CEH liquids could be due to the evaporation of unreacted TEOS (b.p. 168 °C). The addition of the silyl groups could have hindered the condensation reaction between TEOS and the hydroxyl groups from the dissolved silica.

The differences in mass loss were less apparent between CMH and CEH (Figure 7). The TMOS and TEOS concentrations were less than that of the CM and CE liquids. Therefore, the mass difference in the condensed methanol and ethanol had less of an impact to the change in mass. All transitions occurred at the same temperatures between the two liquid precursors.

CMH liquid was chosen to produce a join. The thermal analyses showed that the CMH liquid required the lowest temperature for alcohol producing condensation reactions to occur. The condensation reaction onset temperature

(67 °C) was chosen as the joining temperature. The rate of reaction at the onset temperature could be sufficiently slow for the precursor to remain a liquid and allow volatiles to escape.

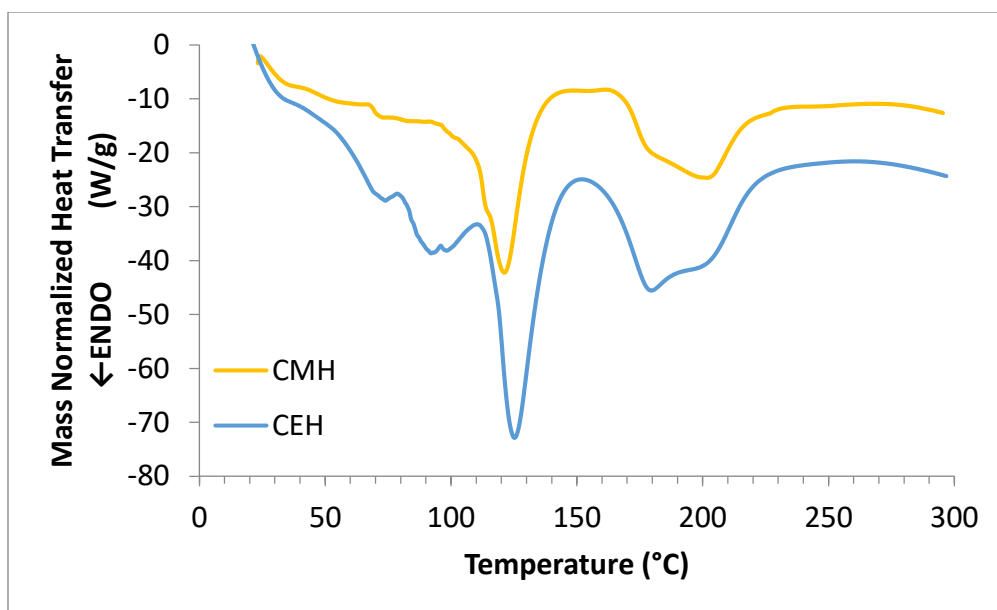


Figure 6. DSC analyses of CMH and CEH precursors.

**3.1.2. Bonded Specimen.** The DSC analysis of the solid CMH showed two endothermic peaks at 90 °C (peak) and 198 °C (peak). When compared to the liquid CMH DSC analysis (Figure 8), the endothermic peak attributed to evaporation of water produced by condensation reactions (200 °C peak) of silanol groups that remained after solidification. The presence of a fishy odor indicated that first endothermic peak was likely from the decomposition of ChOH. In the absence of a stabilizing solvent, ChOH is unstable and can spontaneously decompose at low temperatures<sup>13</sup>. The decomposition temperature of ChOH is

90 °C in the presence of methanol. Therefore, evaporation of methanol from solidification drives the decomposition of ChOH to lower temperatures.

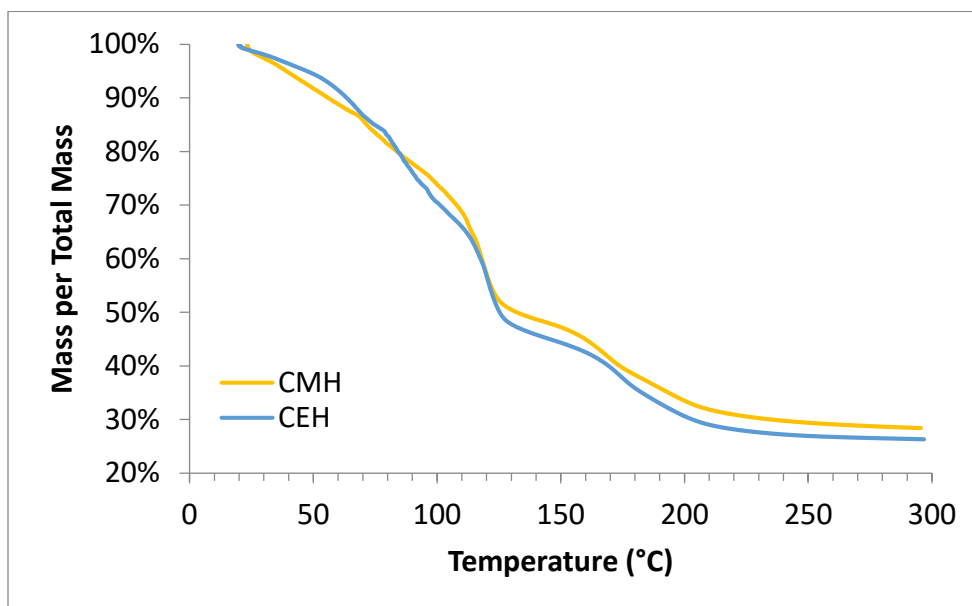


Figure 7. TGA analyses of CMH and CEH precursors.

The TGA analyses of the liquid CMH and solid CMH showed that solidification of the precursor decreased the amount of mass lost up to 300 °C (Figure 9). The solid CMH retained 75% of its original mass at 150 °C while the liquid CMH retained 47%. The difference in mass at 150 °C matched the theoretical mass change due to evaporation of solvent and condensation products. From 150 °C to 300 °C, the solid CMH mass decreased 38%, which is higher than the theoretical mass loss from water produced by condensation reactions (25%). This indicated that the second endothermic peak cannot be attributed solely to water loss. The peak was present in the ChOH-Silica analysis,

therefore it must be due to decomposition and loss of  $\text{CH}_3\text{OH}$ . However, the decomposition products of  $\text{CH}_3\text{OH}$  are reported to evaporate at temperatures lower than  $150\text{ }^\circ\text{C}$ <sup>12</sup>.

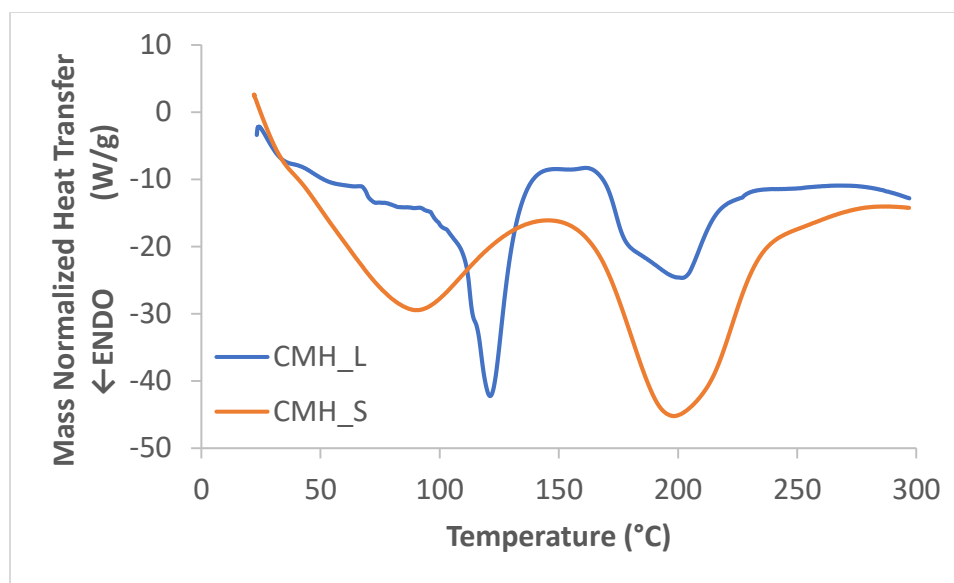


Figure 8. DSC analyses of CMH liquid (CMH\_L) and CMH solid (CMH\_S).

### 3.2. RAMAN SPECTROSCOPY

The Raman spectra of solid and liquid CMH are compared in Figure 10. The liquid CMH Raman spectrum had three peaks at  $525$ ,  $589$ , and  $609\text{ cm}^{-1}$  that were not present in the solid CMH spectrum. The peak at  $525\text{ cm}^{-1}$  was attributed to the stretching mode of a Si-O-Si where one of the silicon atoms is bonded to two alkoxy or silanol groups and the other contains three siloxane bonds. The  $589\text{ cm}^{-1}$  and  $609\text{ cm}^{-1}$  peaks were stretching modes of the Si-O-Si between an alkoxy silane and a silicon with three siloxane bonds (Figure 11)<sup>14</sup>. The

appearance of the three peaks in the liquid CMH spectrum indicated that condensation reactions occurred at room temperature before solidification.

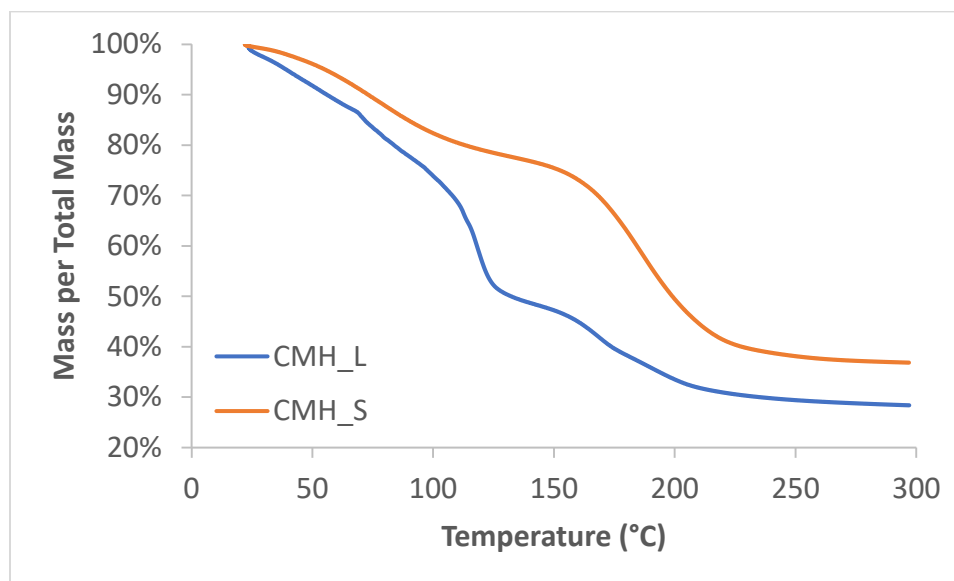


Figure 9. TGA analysis of CMH liquid (CMH\_L) and CMH solid (CMH\_S).

The alkoxy silane molecules formed siloxane bonds with the cubic octasilicate molecules from the dissolution of silica in the ChOH in the liquid. However, the Raman peaks characteristic of a large silica network at  $830\text{ cm}^{-1}$  ( $\text{SiO}_4$  symmetric stretching) and  $1070\text{ cm}^{-1}$  ( $\text{SiO}_4$  asymmetric stretching) were not present in the liquid CMH spectrum indicating that the silica molecules were small. After the liquid solidified, the peaks corresponding to the alkoxy silanes bonding to the cubic octasilicate molecules were not present, which indicated the formation of a three-dimensional silica network. Like the liquid CMH, the solid CMH spectrum did not contain a well-defined  $\text{SiO}_4$  asymmetric stretching peak.

The absence of this peak could indicate that the solidified CMH did not have a continuous siloxane bonded three-dimensional silica network.

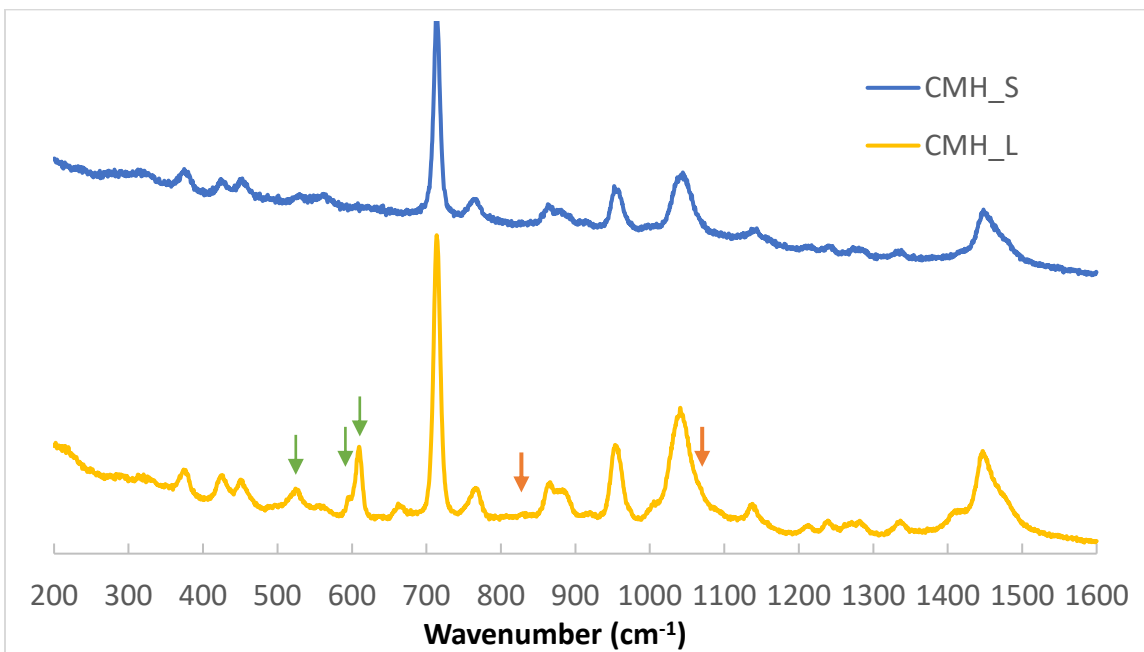


Figure 10. Raman spectra of CMH solid and CMH liquid; alkoxy silane peaks at 525, 589, and 609  $\text{cm}^{-1}$  (green), 3-dimensional silica network peaks at 830 and 1080  $\text{cm}^{-1}$  (orange).

### 3.3. UV-VIS CHARACTERIZATION

The specimen bonded with CMH precursor at 67 °C showed good optical transparency (Figure 12). When the bonded specimen was examined using optical microscopy, the center of the joint contained pores ranging from 7-25  $\mu\text{m}$  in diameter (Figure 13). The UV-VIS spectrum indicated transmission >80% at wavelengths between 350 and 1100 nm (Figure 14).



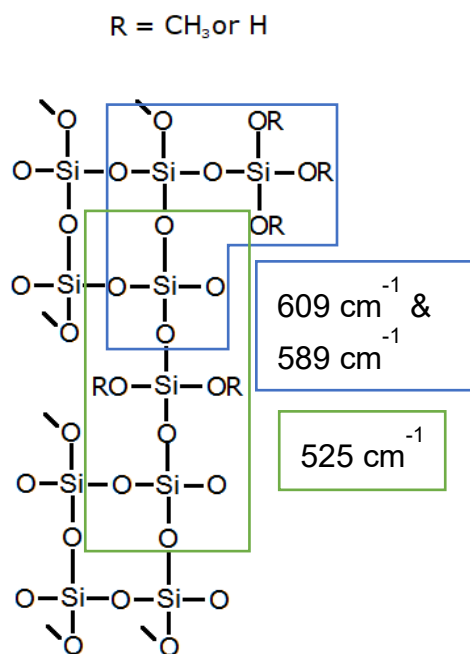


Figure 11. Schematic representation of cross-linking structures and corresponding Raman vibrational modes.



Figure 12. Specimen bonded with CMH liquid precursor at 67 °C.

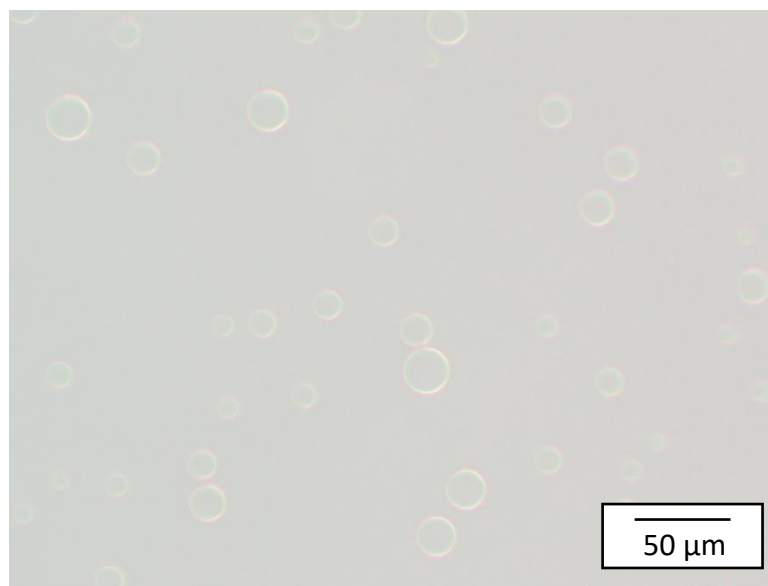


Figure 13. An optical micrograph of the center of the specimen joined with CMH liquid at 67 °C.

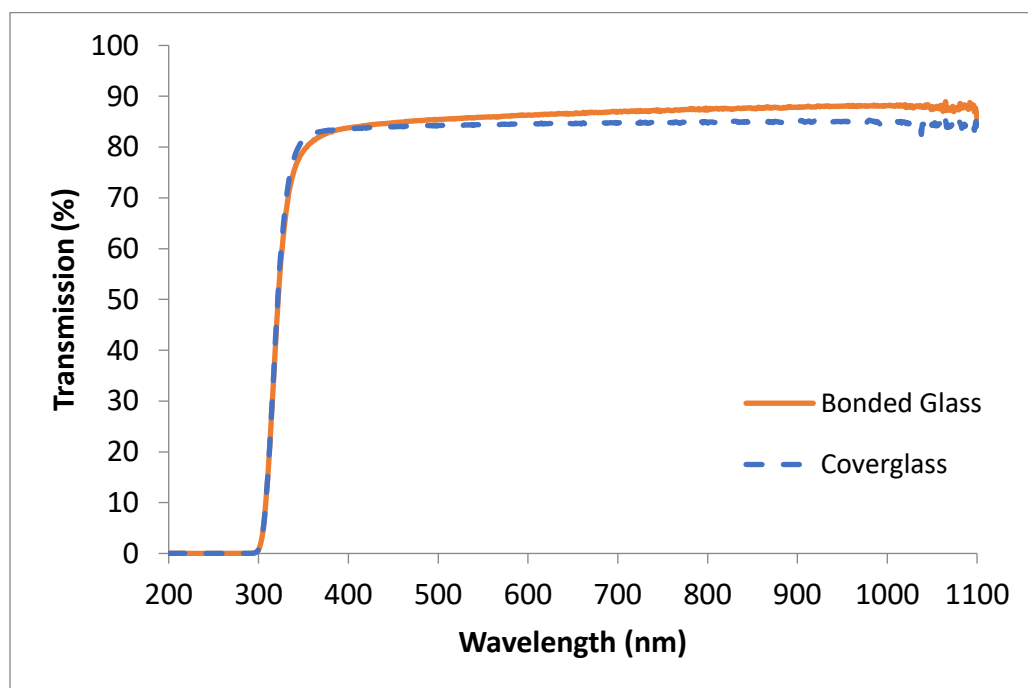


Figure 14. UV-Vis spectra of CMH bonded glass and two unbonded coverglass slides.

Compared to a control specimen consisting of two unbonded borosilicate coverglasses, the bonded specimen had higher transmission in the optical wavelengths. Replacing the air gap between the glass coupons with the joining material reduced the difference between the indices of refraction effectively reducing the reflection of light passing through the specimen.

### 3.4. ISOTHERMAL HOLDS

After heat treatment, all of the CMH-bonded specimens exhibited some degree of discoloration on the perimeter of the join (Figure 15). The discoloration at temperatures lower than 120 °C was likely due to decomposition of unstable  $\text{CHOH}$ , which produces trimethylamine and acetaldehyde. Any acetaldehyde left behind would cause brown discoloration.

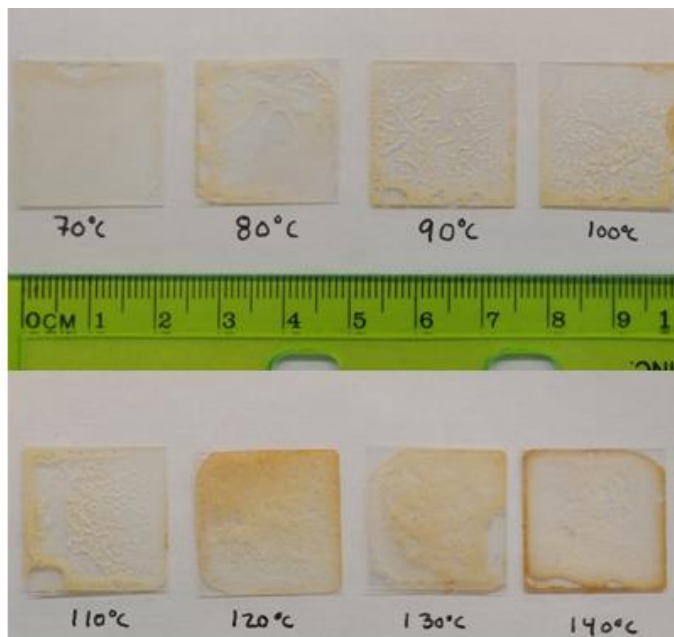


Figure 15. Bonded specimens after 1-hour isothermal holds at specified temperature.

At 120 °C, the specimen had reached the decomposition temperature of ChOH, which caused the discoloration to become more pronounced. The specimens held at temperatures greater than 70 °C also had enlarged pores (Figure 15). The DSC (Figure 8) and TGA (Figure 9) analyses of the solid CMH showed that there was at least a 20% mass loss at 80 °C which led to enlarged pores.

#### 4. CONCLUSIONS

Choline hydroxide-silica solutions were investigated to join borosilicate glass at low temperatures. Alkoxysilanes and hexamethyldisilazane were added to the choline-hydroxide silica solution to form a continuous silica network. Thermal analyses of liquid precursors of various compositions were performed to identify possible joining temperatures. DSC/TGA analyses showed that alcohol condensation reactions occurred at temperatures as low as 67 °C in the choline hydroxide-silica-tetramethoxysilane-hexamethyldisilazane (CMH) liquid precursor. The Raman spectrum of the solidified CMH showed the disappearance of peaks attributed to alkoxy groups. Borosilicate glass coverglasses were bonded with CMH liquid precursor at 67 °C for 20 hours. The bonded CMH specimen exhibited high transmission at wavelengths between 350 and 1100 nm. One-hour isothermal holds of bonded specimens showed the CMH solid has low temperature (<80 °C) stability.

The reported process produced a join between the borosilicate glass coupons. Although the join appeared to be a homogenous solid, the Raman spectrum of the solid CMH did not contain the peaks to suggest the presence of an inorganically bonded network. Hydrogen bonding between the unreacted silanol groups could have produced the rigid gel. The rigid gel could produce a sufficiently strong adhesive layer between the borosilicate glass coupons.

## REFERENCES

- 1 V. Dragoi, "Wafer Bonding Using Spin-On Glass as Bonding Material," pp. 19–32 in *Handb. Wafer Bond*. Edited by P. Ramm, J.-Q. Lu and V. Taklo. Wiley-VCH Verlag & Co. KGaA, Weinheim, Germany, 2012.
- 2 C. Tao, H. Yan, X. Yuan, Q. Yin, J. Zhu, W. Ni, L. Yan, and L. Zhang, "Detailed Analysis and Formation Mechanism of Superhydrophobic Antireflective Coatings with Adjustable Refractive Index from Trimethylsilanized Silica Nanoparticles," *J. Sol-Gel Sci. Technol.*, **80** [1] 10–18 (2016).
- 3 J.A. Burg, M.S. Oliver, T.J. Frot, M. Sherwood, V. Lee, G. Dubois, and R.H. Dauskardt, "Hyperconnected Molecular Glass Network Architectures with Exceptional Elastic Properties," *Nat. Commun.*, **8** [1] 1–8 (2017).
- 4 G. San Vicente, R. Bayón, N. Germán, and A. Morales, "Surface Modification of Porous Antireflective Coatings for Solar Glass Covers," *Sol. Energy*, **85** [4] 676–680 (2011).
- 5 P. Bankovic, N.R. Demarquette, and M.L.P. Da Silva, "Obtention of Selective Membranes for Water and Hydrophobic Liquids by Plasma Enhanced Chemical Vapor Deposition on Porous Substrates," *Mater. Sci. Eng. B Solid-State Mater. Adv. Technol.*, **112** [2–3 SPEC. ISS.] 165–170 (2004).

- 6 H. Ye, X. Zhang, Y. Zhang, L. Ye, B. Xiao, H. Lv, and B. Jiang, "Preparation of Antireflective Coatings with High Transmittance and Enhanced Abrasion-Resistance by a Base/Acid Two-Step Catalyzed Sol-gel Process," *Sol. Energy Mater. Sol. Cells*, **95** [8] 2347–2351 (2011).
- 7 C. Tao, H. Yan, X. Yuan, Q. Yin, J. Zhu, W. Ni, L. Yan, and L. Zhang, "Sol-gel Based Antireflective Coatings with Superhydrophobicity and Exceptionally Low Refractive Indices Built from Trimethylsilylated Hollow Silica Nanoparticles," *Colloids Surfaces A Physicochem. Eng. Asp.*, **509** 307–313 (2016).
- 8 H.M. Shang, Y. Wang, S.J. Limmer, T.P. Chou, K. Takahashi, and G.Z. Cao, "Optically Transparent Superhydrophobic Silica-Based Films," *Thin Solid Films*, **472** [1–2] 37–43 (2005).
- 9 J. Tian, S.K. Deng, and P.Z. Yang, "Optimization of Porous SiO<sub>2</sub> Antireflective (AR) Coatings Used in Encapsulating Solar Modules," *Adv. Mater. Res.*, **739** 94–100 (2013).
- 10 R.K. Iler, "The Chemistry of Silica: Solubility, Polymerization, Colloid and Surface Properties;" pp. 62–64 in 1979.
- 11 I. Hasegawa and S. Sakka, "Formation of CH<sub>3</sub>Si<sub>8</sub>O<sub>19</sub><sup>7-</sup> Cubic Octameric Anion in (2-Hydroxyethyl)trimethylammonium Silicate Aqueous Solutions Containing Hydrolysis Products of Methyltriethoxysilane," *Bull. Chem. Soc. Jpn.*, **63** 3203–3208 (1990).
- 12 K. Haerens, E. Matthijs, K. Binnemans, and B. Van der Bruggen, "Electrochemical Decomposition of Choline Chloride Based Ionic Liquid Analogues," *Green Chem.*, **11** [9] 1357 (2009).
- 13 K. Moonen, D. Ulrichs, and D. Scheldemen, Process for Choline Hydroxide; 14/783143, 2016.
- 14 C.J. Brinker and G.W. Scherer, *Sol-Gel Science: The Physics and Chemistry of Sol-Gel Processing*. 1990.

## SECTION

### 3. CONCLUSIONS

The purpose of this project was to develop possible techniques for producing a thermally-stable, optically transparent join between borosilicate glass and a PV cell at temperatures below 200 °C. A joining technique that used deep eutectic solvents was investigated to determine processing parameters that produce a join. Choline hydroxide was investigated as a way of incorporating silica into the join using a different joining technique.

#### 3.1. PAPER I CONCLUSIONS

This study investigated deep eutectic solvents to join borosilicate glass to inorganic substrates by increasing the silica concentration and melting temperature of the join. The conclusions from this study were:

- A join produced using this technique was an amorphous silica-based organic-inorganic hybrid.
- Dissolved silica and alumina concentrations were not adequate for creating an inorganic join.
- Joining borosilicate glass coupons was unsuccessful at temperatures between 100-150 °C.
- Altering the oxygen partial pressure did not have a significant effect on the success of the join.

### 3.2. PAPER II CONCLUSIONS

This study investigated a low temperature sol-gel processing technique to produce a join between borosilicate glass coupons using choline hydroxide to increase the initial silica concentration. The conclusions from this study were:

- Alcohol condensation reactions occur at 67 °C for liquid precursors containing choline hydroxide-silica, tetramethoxysilane, and hexamethyldisilazane.
- An optically transparent join was produced when joined at 67 °C for 20 hours.
- The solid produced was not a completely inorganically bonded network.
- The join was not thermally stable at temperatures <80 °C

### 3.3. OVERALL CONCLUSIONS

High silica concentrations are required for producing a successful join between borosilicate glass substrates. Deep eutectic solvents do not produce solutions with adequate silica concentrations for joining borosilicate glass at low temperatures. Although choline hydroxide can produce a solution with a sufficient silica concentration to join borosilicate glass, the decomposition of choline hydroxide causes discoloration of the join at low temperatures.



## 4. SUGGESTIONS FOR FUTURE WORK

### 4.1. THERMAL STABILITY

The joins produced from the choline hydroxide methanol solution were optically transparent at low temperatures. However, the decomposition of choline hydroxide caused the join to turn brown at 80 °C. The thermal stability could be improved by reacting the choline hydroxide with a chloride species to produce choline chloride which has a decomposition temperature of 285 °C. Additions of chlorosilanes could produce choline chloride and incorporate cross-linking components.

Choline hydroxide could be replaced with a different quaternary ammonium hydroxide to improve thermal stability. Silica exhibits a solubility of 41% by weight in tetramethylammonium hydroxide<sup>20</sup> and has a decomposition temperature of 135°C. The decomposition products are trimethylamine, methanol and dimethylether<sup>64</sup> gases. The absence of a solid decomposition product could decrease the chance of discoloration in the join. However, the decomposition could cause an increase in volume shrinkage and delamination of the join from the substrates.

### 4.2. MECHANICAL TESTING

The solidified join requires mechanical testing. The join-borosilicate glass adhesion strength can be tested using a double-lap shear test<sup>65</sup> and the elastic modulus of the joined specimen can be tested using four-point flexural testing<sup>66</sup>.

The adhesion strength and elastic modulus values can be compared to values for optical silicones to determine the relative improvement of the mechanical characteristics.

The mechanical properties could be improved with the addition of metal oxides. Alumina exhibits high solubilities in strong bases and could increase the elastic modulus of join<sup>67</sup>. The effect of the alumina concentration on the elastic modulus values can be determined by four-point flexural testing.

## BIBLIOGRAPHY

- 1 P. Patel, D. Aiken, A. Boca, B. Cho, D. Chumney, M.B. Clevenger, A. Cornfeld, N. Fatemi, *et al.*, "Experimental Results from Performance Improvement and Radiation Hardening of Inverted Metamorphic Multijunction Solar Cells," *IEEE J. Photovoltaics*, **2** [3] 377–381 (2012).
- 2 J.S. Stroud, "Photoionization of  $Ce^{3+}$  in Glass," *J. Chem. Phys.*, **35** [3] 844–850 (1961).
- 3 P. Ramm, J.-Q. Lu, M. Maaïke, and V. Taklo, *Handbook of Wafer Bonding*. 2012.
- 4 E. Orowan, "Fracture and Strength of Solids," *Rep. Prog. Phys.*, **12** 185–230 (1949).
- 5 T. Kawaguchi, J. Iura, N. Taneda, H. Hishikura, and Y. Kokubu, "Structural Changes of Monolithic Silica Gel During the Gel-to-Glass Transition," **82** 50–56 (1986).
- 6 H. Ye, X. Zhang, Y. Zhang, L. Ye, B. Xiao, H. Lv, and B. Jiang, "Preparation of Antireflective Coatings with High Transmittance and Enhanced Abrasion-Resistance by a Base/Acid Two-Step Catalyzed Sol-gel Process," *Sol. Energy Mater. Sol. Cells*, **95** [8] 2347–2351 (2011).
- 7 A.P. Abbott, G. Capper, D.L. Davies, H.L. Munro, R.K. Rasheed, and V. Tambyrajah, "Preparation of Novel, Moisture-Stable, Lewis-Acidic Ionic Liquids Containing Quaternary Ammonium Salts With Functional Side Chains," *Chem. Commun.*, [19] 2010–2011 (2001).
- 8 A. P. Abbott, D. Boothby, G. Capper, D.L. Davies, and R. Rasheed, "Deep Eutectic Solvents Formed Between Choline Chloride and Carboxylic Acids," *J. Am. Chem. Soc.*, **126** [9] 9142 (2004).
- 9 A.P. Abbott, J.C. Barron, G. Frisch, S. Gurman, K.S. Ryder, and A. Fernando Silva, "Double Layer Effects on Metal Nucleation in Deep Eutectic Solvents," *Phys. Chem. Chem. Phys.*, **13** [21] 10224 (2011).
- 10 A.P. Abbott, K. El Ttaib, G. Frisch, K.J. McKenzie, and K.S. Ryder, "Electrodeposition of Copper Composites from Deep Eutectic Solvents Based on Choline Chloride," *Phys. Chem. Chem. Phys.*, **11** [21] 4269 (2009).

- 11 A.P. Abbott, K. El Ttaib, G. Frisch, K.S. Ryder, and D. Weston, "The Electrodeposition of Silver Composites Using Deep Eutectic Solvents," *Phys. Chem. Chem. Phys.*, **14** [7] 2443 (2012).
- 12 A.P. Abbott, G. Capper, D.L. Davies, K.J. McKenzie, and S.U. Obi, "Solubility of Metal Oxides in Deep Eutectic Solvents Based on Choline Chloride," *J. Chem. Eng. Data*, **51** [4] 1280–1282 (2006).
- 13 Z. Ma, J.H. Yu, and S. Dai, "Preparation of Inorganic Materials Using Ionic Liquids," *Adv. Mater.*, **22** [2] 261–285 (2010).
- 14 K. Haerens, E. Matthijs, K. Binnemans, and B. Van der Bruggen, "Electrochemical Decomposition of Choline Chloride Based Ionic Liquid Analogues," *Green Chem.*, **11** [9] 1357 (2009).
- 15 C.J. Brinker and G.W. Scherer, *Sol-Gel Science: The Physics and Chemistry of Sol-Gel Processing*. 1990.
- 16 J.C. Pouxviel, J.P. Boilot, O. Poncelet, L.G. Hubert-Pfalzgraf, A. Lecomte, A. Dager, and J.C. Beloeil, "An Aluminosiloxane as a Ceramic Precursor," *J. Non. Cryst. Solids*, **93** [2–3] 277–286 (1987).
- 17 J. Livage, M. Henry, and C. Sanchez, "Sol-gel Chemistry of Transition Metal Oxides," *Prog. Solid State Chem.*, **18** [4] 259–341 (1988).
- 18 R.E. Timms, "Five-Co-Ordinate Silicon: Kinetics of the Acid-Catalyzed Hydrolysis of Nitrotripenoxysilanes," *J. Chem. Soc.*, 1969–1974 (1971).
- 19 R.K. Iler, "The Chemistry of Silica: Solubility, Polymerization, Colloid and Surface Properties," pp. 62–64 in 1979.
- 20 M. Yamane, S. Inoue, and A. Yasumori, "Sol-gel Transition in the Hydrolysis of Silicon Methoxide," *J. Non. Cryst. Solids*, **63** [1–2] 13–21 (1984).
- 21 S.N. Laboratories, "Sol-gel Transition in Simple Silicates II," *J. Non. Cryst. Solids*, **63** [1–2] 45–59 (1984).
- 22 G.. Young, "Interaction of Water Vapor with Silica Surfaces," *J. Colloid Sci.*, **13** [1] 67–85 (1958).
- 23 G.. Young and T.P. Bursh, "Immersion Calorimetry Studies of the Interaction of Water with Silica Surfaces," *J. Colloid Sci.*, **15** 361–369 (1960).

- 24 S.P. Zhdanov, "Liberation of Hydrogen in the Roasting of Quartz," *Bull. Acad. Sci. USSR div. Chem. Sci.*, **8** [2] 326–327 (1959).
- 25 G. Curthoys, V.Y. Davydov, A. V. Kiselev, S.A. Kiselev, and B. V. Kuznetsov, "Hydrogen Bonding in Adsorption on Silica," *J. Colloid Interface Sci.*, **48** [1] 58–72 (1974).
- 26 C. Okkerse, "Porous Silica," p. 214 in *Phys. Chem. Asp. Adsorbents Catal.* 1970.
- 27 D. Barby, "Silicas," p. 353 in *Charact. Powder Surfaces.* 1976.
- 28 M.M. Dubinin, B.P. Bering, and V.V. Serpinskii, *Recent Progress in Surface Science.* 1964.
- 29 N.H. Ceaglske and O.A. Hougen, "Drying Granular Solids," *Ind. Eng. Chem.*, **29** [7] 805–813 (1937).
- 30 E.P. Plueddemann, *Silanes, Surfaces, and Interfaces.* Gordon and Breach, Amsterdam, 1986.
- 31 C. Tao, H. Yan, X. Yuan, Q. Yin, J. Zhu, W. Ni, L. Yan, and L. Zhang, "Sol-gel Based Antireflective Coatings with Superhydrophobicity and Exceptionally Low Refractive Indices Built from Trimethylsilanized Hollow Silica Nanoparticles," *Colloids Surfaces A Physicochem. Eng. Asp.*, **509** 307–313 (2016).
- 32 H.M. Shang, Y. Wang, S.J. Limmer, T.P. Chou, K. Takahashi, and G.Z. Cao, "Optically Transparent Superhydrophobic Silica-Based Films," *Thin Solid Films*, **472** [1–2] 37–43 (2005).
- 33 G. San Vicente, R. Bayón, N. Germán, and a. Morales, "Surface Modification of Porous Antireflective Coatings for Solar Glass Covers," *Sol. Energy*, **85** [4] 676–680 (2011).
- 34 P. Bankovic, N.R. Demarquette, and M.L.P. Da Silva, "Obtention of Selective Membranes for Water and Hydrophobic Liquids by Plasma Enhanced Chemical Vapor Deposition on Porous Substrates," *Mater. Sci. Eng. B Solid-State Mater. Adv. Technol.*, **112** [2–3 SPEC. ISS.] 165–170 (2004).
- 35 Y. Haruvy and S.E. Webber, "Supported Sol–Gel Thin-Film Glasses Embodying Laser Dyes. 1. A New Fast Method for the Preparation of Optically Clear Polysiloxane Thin-Film Glasses," *Chem. Mater.*, **3** [3] 501–507 (1991).

- 36 C. Okkerse, *Submicroporous and Macroporous Silica*. Delftsche Uitgevers Maatschappij N.V. Delft, 1961.
- 37 W.C. Beard, "Infrared Studies of Aqueous Silicate Solutions;" pp. 162–168 in *Mol. Sieves*. 1973.
- 38 I. Hasegawa and S. Sakka, "Formation of  $\text{CH}_3\text{Si}_8\text{O}_{19}^{7-}$  Cubic Octameric Anion in (2-Hydroxyethyl)trimethylammonium Silicate Aqueous Solutions Containing Hydrolysis Products of Methyltriethoxysilane," *Bull. Chem. Soc. Jpn.*, **63** 3203–3208 (1990).
- 39 R.H. Baney, M. Itoh, A. Sakakibara, and T. Suzuki, "Silsesquioxanes," *Chem. Rev.*, **95** [5] 1409–1430 (1995).
- 40 X. Zhang, W. Lin, J. Zheng, Y. Sun, B. Xia, L. Yan, and B. Jiang, "Insight into the Organic–Inorganic Hybrid and Microstructure Tailor Mechanism of Sol–Gel ORMOSIL Antireflective Coatings," *J. Phys. Chem. C*, **122** [1] 596–603 (2018).
- 41 C. Tao, H. Yan, X. Yuan, Q. Yin, J. Zhu, W. Ni, L. Yan, and L. Zhang, "Detailed Analysis and Formation Mechanism of Superhydrophobic Antireflective Coatings with Adjustable Refractive Index from Trimethylsilanized Silica Nanoparticles," *J. Sol-Gel Sci. Technol.*, **80** [1] 10–18 (2016).
- 42 J.A. Burg, M.S. Oliver, T.J. Frot, M. Sherwood, V. Lee, G. Dubois, and R.H. Dauskardt, "Hyperconnected Molecular Glass Network Architectures with Exceptional Elastic Properties," *Nat. Commun.*, **8** [1] 1–8 (2017).
- 43 F. Hoffmann, M. Cornelius, J. Morell, and M. Fröba, "Silica-Based Mesoporous Organic-Inorganic Hybrid Materials," *Angew. Chemie - Int. Ed.*, **45** [20] 3216–3251 (2006).
- 44 J. Wen and G.L. Wilkes, "Organic-Inorganic Hybrid Network Materials by the Sol-gel Approach," *Chem. Mater.*, **8** [8] 1667–1681 (1996).
- 45 J.D. Mackenzie, "Structures and Properties of Ormosils," *J. Sol-Gel Sci. Technol.*, **2** [1–3] 81–86 (1994).
- 46 R. Knechtel, "Glass Frit Wafer Bonding;" pp. 3–17 in *Handb. Wafer Bond*. Edited by P. Ramm, J.-Q. Lu and V. Taklo. Wiley-VCH Verlag & Co. KGaA, Weinheim, Germany, 2012.
- 47 R. Knechtel, "Glass frit bonding: An Universal Technology for Wafer Level Encapsulation and Packaging," *Microsyst. Technol.*, **12** [1–2 SPEC. ISS.] 63–68 (2005).

- 48 A. Kaur, A. Khanna, S. Singla, A. Dixit, G.P. Kothiyal, K. Krishnan, S.K. Aggarwal, V. Sathe, *et al.*, "Structure-Property Correlations in Lead Silicate Glasses and Crystalline Phases," *Phase Transitions*, **86** [8] 759–777 (2013).
- 49 P.D. CALVERT and R.R. SHAW, "Liquidus Behavior in the Silica-Rich Region of the System PbO-SiO<sub>2</sub>," *J. Am. Ceram. Soc.*, **53** [6] 350–352 (1970).
- 50 J.E. Shelby, *Introduction to Glass Science and Technology*. The Royal Society of Chemistry, Cambridge, UK, 2005.
- 51 V. Dragoi, "Wafer Bonding Using Spin-On Glass as Bonding Material;" pp. 19–32 in *Handb. Wafer Bond.* Edited by P. Ramm, J.-Q. Lu and V. Taklo. Wiley-VCH Verlag & Co. KGaA, Weinheim, Germany, 2012.
- 52 H.C. Lin, K.L. Chang, G.W. Pickrell, K.C. Hsieh, and K.Y. Cheng, "Low Temperature Wafer Bonding by Spin On Glass," *J. Vacuum Sci. Technol.*, **20** [2] 752–754 (2002).
- 53 V. Dragoi, "Si/GaAs Heterostructures Fabricated by Direct Wafer Bonding," *MRS Proc.*, **681** 73–78 (2001).
- 54 F. Niklaus and J.-Q. Lu, "Polymer Adhesive Wafer Bonding;" pp. 33–58 in *Handb. Wafer Bond.* Edited by P. Ramm, J.-Q. Lu and V. Taklo. Wiley-VCH Verlag & Co. KGaA, Weinheim, Germany, 2012.
- 55 E.W. Flick, *Adhesives, Sealants and Coatings for the Electronic Industry*. Noyes Publications, Park Ridge, NJ, 1986.
- 56 F. Niklaus, G. Stemme, J.Q. Lu, and R.J. Gutmann, "Adhesive Wafer Bonding," *J. Appl. Phys.*, **99** [3] (2006).
- 57 W.M. Alvino, *Plastics for Electronics: Materials, Properties, and Design*. McGraw-Hill, New York, NY, 1995.
- 58 C. Nobel, *Industrial Adhesives Handbook*. Casco Nobel, Fredensborg, Denmark, 1992.
- 59 W. Brostow, "Mechanical Properties;" pp. 423–446 in *Phys. Prop. Polym. Handb.* Edited by J.E. Mark. Springer Science, New York, NY, 2007.
- 60 M.G. Nicholas, *Joining Processes: Introduction to Brazing and Diffusion Bonding*. Kluwer Academic Publishers, Glasgow, UK, 1998.

- 61 M.M. Schwartz, *Ceramic Joining*. ASM International, Materials Park, OH, 1990.
- 62 K.P. Trumble, "Prediction of a Critical Temperature for Aluminate Formation in Alumina / Copper – Oxygen Eutectic Bonding," *J. Am. Ceram. Soc.*, **82** [10] 2919–2920 (1999).
- 63 W.K. Musker, "A Reinvestigation of the Pyrolysis of Tetramethylammonium Hydroxide," *J. Am. Chem. Soc.*, **86** [5] 960–961 (1964).
- 64 ASTM.D3528-96(2016), "Standard Test Method for Strength Properties of Double Lap Shear Adhesive Joints by," *ASTM Int.*, **96** [Reapproved 2016] 6–9 (2016).
- 65 F. Carrillo, S. Gupta, M. Balooch, S.J. Marshall, G.W. Marshall, L. Pruitt, and C.M. Puttlitz, "Nanoindentation of Polydimethylsiloxane Elastomers: Effect of Crosslinking, Work of Adhesion, and Fluid Environment on Elastic Modulus," *J. Mater. Res.*, **20** [10] 2820–2830 (2005).
- 66 R.J. Eagan and J.C. Swearingen, "Effect of Composition on the Mechanical Properties of Aluminosilicate and Borosilicate Glasses," *J. Am. Ceram. Soc.*, **61** [1–2] 27–30 (1978).



## VITA

Eric Muskovin was born in Muskegon, Michigan. He received his Bachelor of Science in Ceramic Engineering from Missouri University of Science and Technology in May 2016.

He started his Master of Science in Material Science and Engineering at Missouri University of Science and Technology in June 2016. His areas of interest are in ceramic and glass chemistries.

Eric Muskovin worked as a graduate research assistant for two years in the Material Science and Engineering Department at Missouri University of Science and Technology.

In July 2018 he received his Master of Science in Materials Science and Engineering from Missouri University of Science and Technology.